

Aus der Klinik für Augenheilkunde
Direktor: Prof. Dr. med. B. Seitz, F.E.B.O.
Universitätsklinikum des Saarlandes UKS
Homburg/Saar

Experimentelle Hornhautbildgebung und Hornhautchirurgie mit Femtosekundenlaserpulsen

**Experimental corneal imaging and corneal surgery with
femtosecond laser pulses**

*Dissertation zur Erlangung des Grades eines Doktors der Medizin
der Medizinischen Fakultät
der UNIVERSITÄT DES SAARLANDES*

2012

vorgelegt von

Corinne Huss

geb. am 29.06.1980 in Ettelbruck, Luxembourg

Table of contents

Abbreviations	4
1. Summary / Zusammenfassung	6
1.1. Summary	6
1.2. Zusammenfassung	8
2. Introduction	10
2.1. Corneal anatomy	10
2.2. Corneal pathology	11
2.2.1. Fuchs' endothelial dystrophy	11
2.2.2. Keratoconus	12
2.2.3. Herpes simplex virus keratitis	12
2.3. The clinical examination of the cornea	13
2.4. Refractive surgery: a historical overview	14
2.5. Multiphoton laser scanning microscopy	17
2.6. Laser-tissue interactions	19
2.7. Aims of the study	19
3. Materials and Methods	20
3.1. Corneal samples	20
3.1.1. Acquisition and treatment before the laser experiment	20
3.1.1.1. Porcine corneas	20
3.1.1.2. Human corneas	20
3.1.2. Treatment after the laser experiment	21
3.2. System configurations	22
3.3. Choice of scanning time	24
4. Results	26
4.1. Imaging cornea without pathology	26
4.1.1. Epithelium	27
4.1.2. Stroma	27

	3
4.1.2.1. Autofluorescence	27
4.1.2.2. Second harmonic generation	27
4.1.2.3. Morphological intrastromal observations	32
4.2. Imaging pathologic human cornea	33
4.2.1. Keratoconus	33
4.2.2. Fuchs' endothelial dystrophy	39
4.2.3. Herpes simplex virus keratitis	44
4.3. Cutting of corneal tissue	47
4.3.1. Morphology	47
4.3.2. Dependence of lesion width on tissue depth	50
4.3.3. Dependence of lesion width on pulse energy	51
5. Discussion	53
5.1. Cornea imaging using autofluorescence and second harmonic generation	53
5.2. Imaging pathological cornea	55
5.3. Linear tissue ablation	56
5.4. Conclusion	58
6. References	60
7. Publikationen	63
8. Danksagung	64

Abbreviations

AF	autofluorescence
ArF	argon fluorine
c	speed of light
DALK	deep anterior lamellar keratoplasty
DMEK	Descemet membrane endothelial keratoplasty
DSAEK	Descemet stripping automated endothelial keratoplasty
E_0	dielectric constant
E.g.	exempli gratia
Fig.	figure
Fs	femtosecond
Hrs	hours
HRT	Heidelberg Retina Tomograph
HSV	herpes simplex virus
KP	Kurypass (shortpass)
λ	light wave length
LASEK	laser-assisted subepithelial keratectomy
LASIK	laser-assisted in situ keratomileusis
LSM	laser scanning microscope
M	molar
N	number of trials
NA	numerical aperture
NAD(P)H	nicotinamide adenine (phosphate) dinucleotide (reduced form)
OCT	optical coherence tomography
PERK	prospective evaluation of radial keratotomy
PMT	photomultiplier tube
PRK	photorefractive keratectomy
ROI	region of interest
SHG	second harmonic generation
SL	slit lamp
Tab.	table

UV

ultraviolet

z

tissue depth

1. Summary / Zusammenfassung

1.1. Summary

Purpose: This study employed a non-amplified near-infrared femtosecond laser system for low-invasive, real-time imaging of native corneal tissue at submicron resolution as well as for epithelial and intrastromal tissue modification. The used system consisted of a non-amplified near-infrared femtosecond laser scanning microscope operating at low pulse energies below 2 nJ. The purpose of the study was to examine corneal tissue and to determine morphologic and spectral characteristics in two photon excited autofluorescence and in second harmonic generation. Furthermore, cutting effects in corneal tissue as a function of age and condition of the specimen, laser wavelength, scanning time, tissue depth and power at the target were investigated. Selected corneal samples were studied with light microscopy.

Materials and Methods: Porcine corneal samples were prepared from enucleated bulbi gained at the abattoir. Specimens of pathological human corneas were obtained during penetrating or lamellar keratoplasty. Donor corneas not meeting the requirements for transplantation were also analyzed in this study.

Mode-locked, non-amplified Titanium-Sapphire femtosecond lasers coupled to a laser-scanning microscope were used to image and incise corneal tissue. Lasers coupled to the LSM510-META™ (Zeiss, Jena, Germany) included the Chameleon™ (Coherent Inc., Santa Clara, CA), the Vitesse™ (Coherent Inc., Santa Clara, CA) and the Mai-Tai™ One Box (Spectra Physics, Mountain View, CA). The Chameleon™ laser was also coupled to the DermalInspect™ (Jenlab GmbH, Jena, Germany) tomograph.

Results: Corneal structures were selectively imaged by alternating autofluorescence and second harmonic generation imaging. Autofluorescence images revealed cellular components such as epithelial cells and fibrocytes while second harmonic generation images showed the collagen matrix. Human donor tissue and human recipient tissue obtained during keratoplasty with common corneal pathologies

including Fuchs' endothelial dystrophy, herpes simplex virus keratitis and keratoconus were imaged. Observations were correlated with light microscopy. Linear scanning within the stroma at higher pulse energies led to a highly luminescent plasma along the scanning line (tissue obtained within 8 hrs from the abbatoir) or to a dark line (tissue obtained within 48 hrs from the abbatoir). Lesion widths were below 10 μm . A wavelength of 800 nm and a scan time of 15 s proved to be most effective for intrastromal cutting. Lesion width increased with laser power at the target and decreased with tissue depth. A power threshold of 65 mW at the objective was necessary to cause a visible lesion in the stroma at a tissue depth of 100 μm . Surrounding stroma was intact in light microscopy after performing small lesions.

Conclusions: High resolution, transversal images of corneal tissue permitting the description of subcellular detail were performed. Morphological and spectral characteristics were identified in pathological human corneas. Verification of corneal tissue ablation was possible within seconds by reducing the laser power and the scanning mode. In light microscopy, surrounding stroma appeared intact after linear intrastromal ablation. This might have suggested tissue retraction after cutting. Further studies involving the examination of larger stromal volumes and of unintended effects such as phototoxicity and photobleaching would be necessary.

1.2. Zusammenfassung

Zielsetzung: Diese Studie bediente sich eines unverstärkten, im Nahinfrarotbereich arbeitenden Femtosekundenlasersystems. Das System unterstützte minimal-invasive und Echtzeit-Bildgebung von nativem Hornhautgewebe in submikron-Auflösung und ermöglichte die Bearbeitung von epithelalem und stromalem Gewebe. Es bestand aus einem unverstärkten, im Nahinfrarotbereich arbeitenden Femtosekundenlaser-Scanning-Mikroskop mit Pulsenergien unter 2 nJ. Ziel der Studie war es, Hornhautgewebe zu untersuchen und morphologische und spektrale Eigenschaften anhand von Autofluoreszenz und von Frequenzverdopplung zu beschreiben. Der Gewebeabtrag in der Hornhaut wurde in Abhängigkeit von Alter und Zustand der Probe, von Gewebetiefe, Laserwellenlänge, Scanzeit und Laserleistung an der Probe untersucht. Einige Proben wurden der Lichtmikroskopie unterzogen.

Material und Methoden: Aus im Schlachthof enukleierten Schweineaugen wurden Hornhäute präpariert. Präparate pathologischer, menschlicher Hornhäute wurden im Rahmen perforierender und lamellärer Keratoplastiken gewonnen.

Auch Spenderhornhäute, die den Transplantatanforderungen nicht genügten, wurden untersucht. Systemkonfigurationen, die jeweils einen an ein Laserscanningmikroskop angeschlossenen, modengekoppelten, unverstärkten Titan – Saphir Laser beinhalteten, wurden zur Bildgebung und zum Gewebeabtrag von Hornhautgewebe genutzt. Die Laser Chameleon[®] (Coherent Inc., Santa Clara, CA), Vitesse[®] (Coherent Inc., Santa Clara, CA) und Mai-Tai[®] One Box (Spectra Physics, Mountain View, CA) wurden an ein Laserscanningmikroskop LSM510-META[®] (Zeiss, Jena, Deutschland) gekoppelt. Der Chameleon[®] Laser wurde auch an den DermalInspect[®] (Jenlab GmbH, Jena, Deutschland) Tomographen gekoppelt.

Ergebnisse: Hornhautstrukturen wurden wahlweise mittels Autofluoreszenz und Frequenzverdopplung dargestellt. Bildgebung mittels Autofluoreszenz zeigte zelluläre Bestandteile wie Epithelzellen und Fibrozyten, während Bildgebung mittels Frequenzverdopplung die kollagene Matrix darstellte. Menschliches Spendergewebe und bei Keratoplastiken gewonnenes menschliches Empfängergewebe mit verbreiteten Hornhautpathologien wie Fuchs'sche Endotheldystrophie, Herpes

simplex Virus Keratitis und Keratokonus wurden untersucht. Die Beobachtungen wurden mit der Lichtmikroskopie korreliert. Linearer Gewebeabtrag im Stroma bei höheren Pulsenergien ließ ein lumineszentes Plasma entlang der Scanlinie (im Gewebe, welches innerhalb der letzten 8 Stunden aus dem Schlachthof gewonnen wurde) oder eine dunkle Linie (im Gewebe, welches innerhalb der letzten 48 Stunden aus dem Schlachthof gewonnen wurde) entstehen. Die Läsionsbreiten waren geringer als 10 μm . Eine Wellenlänge von 800 nm und eine Scanzeit von 15 s waren für die intrastromale Gewebearbeitung am besten geeignet. Die Läsionsbreite nahm mit der Laserleistung an der Probe zu und mit zunehmender Gewebetiefe ab. Eine Laserleistung von mindestens 65 mW an der Probe war notwendig, um eine sichtbare Läsion im Stroma in einer Gewebetiefe von 100 μm zu erzeugen. Das umgebende Stroma zeigte sich nach dem Erzeugen kleiner stromaler Läsionen lichtmikroskopisch intakt.

Schlussfolgerungen: Hochauflösende, transversale Bilder von Hornhautgewebe mit subzellulären Details wurden angefertigt. Morphologische und spektrale Charakteristika wurden in pathologischem menschlichem Hornhautgewebe identifiziert. Eine Darstellung der Lasereffekte innerhalb weniger Sekunden erforderte lediglich die Reduktion von Laserleistung und Scanform. Nach linearem intrastromalen Gewebeabtrag war das umgebende Stroma lichtmikroskopisch intakt. Dies liess sich eventuell durch eine Geweberetraktion erklären. Weitere Studien sind erforderlich, in denen grössere Stromavolumina bearbeitet und unerwünschte Wirkungen wie Phototoxizität und Photobleichung untersucht werden.

2. Introduction

2.1. Corneal anatomy

The cornea provides the essential optics of the eye with a focusing power of approximately 43 diopters. Corneal integrity and transparency are required for the protection of the intraocular content and for the focusing of a clear image onto the retina. The cornea consists of several cell layers which involve the epithelium, the basal lamina, Bowman's layer, the stroma, Descemet's membrane and the endothelium. The cornea is avascular and contains sensitive nerves from the nasociliary nerve protruding into the epithelium (37).

Epithelium

The epithelium has a central thickness of approximately 50 μm . The epithelial cells are being regenerated by stem cells located at the limbus and by basal cells capable of mitosis.

The apical squamous cell layer, consisting of broad and flattened cells represents the most anterior cell layer of the cornea. *The multilayered polygonal-shaped wing cells* with large ovoid nuclei are in between apical and basal cells. *The basal cell layer* consisting of elongated and polygonal cells with prominent ovoid nuclei is the most posterior layer adjacent to the basal lamina (44).

Basal membrane

This basal membrane links the epithelial basal cells with Bowman's layer.

Bowman's layer

Bowman's layer has a thickness of 10-20 μm and represents a homogenous acellular layer of the stroma with some tropocollagen filaments (37).

Stroma

The stroma forms the largest part of the cornea with a thickness of approximately 450 μm in the center. It consists mainly of collagen lamellae and ground substance made of proteoglycans forming together the extracellular matrix. The proteoglycans are formed by protein cores covalently bound to glycosaminoglycans (keratan sulphate, dermatan sulphate, chondroitin sulphate, chondroitin and hyaluronic acid). Collagen types are mainly type I, with also types III, V, VI (44). Cellular components

account for 3-5% of the stromal volume and include keratocytes, keratoblasts, nerve axons and some lymphocytes.

Descemet's membrane

Descemet's membrane represents the elastic basal membrane of the endothelium composed of collagen fibrils. Its thickness increases from around 3 μm at birth to around 10 μm in adulthood.

Endothelium

It consists of a single layer of hexagonal cells. Their width is 20 μm and their height is 0.1 – 0.2 μm . On average, approximately 3000 cells / mm^2 form the endothelium in an adult population (49).

2.2. Corneal pathology

2.2.1. Fuchs' endothelial dystrophy

Definition: Fuchs' endothelial dystrophy is a genetic or sporadic disorder leading to a decrease in vision due to endothelial decompensation and subsequent stromal and epithelial oedema.

Epidemiology: The disease inheritance may be autosomal dominant or sporadic, with a higher prevalence among females and in higher age (16).

Clinical signs: Three stages can be distinguished. Stage 1: Cornea guttata is the only clinical finding in the first stage. Guttatae are wart-like accumulations of collagen at the posterior surface of Descemet's membrane. Stage 2: The second stage correlates with endothelial decompensation causing stromal edema and consequently epithelial edema. Vision is blurred particularly in the morning. Stage 3: Persistent epithelial edema and bullous keratopathy define the third stage. Bursting epithelial bullae produce pain due to the exposure of nerve endings. Bowman's layer may be replaced by a subepithelial degenerative partly vascularized pannus in advanced stages.

Therapy: Early stages can be alleviated by dehydration achieved by hypertonic eye drops. As the disease progresses, penetrating keratoplasty or posterior lamellar keratoplasty represents the treatment of choice.

2.2.2. Keratoconus

Definition: Keratoconus is a non-inflammatory ocular disease characterised by conical deformation, progressive thinning and scarring of the central cornea (3).

Epidemiology: The disease is rarely hereditary and mainly sporadic. It can be associated to systemic disorders (Down's syndrome, Marfan etc).

Clinical signs: The first sign of the disease is normally a reduced vision in adolescence due to an irregular astigmatism. The cornea shows a paracentral stromal thinning and a cone-like shape. Keratoconus seems to originate in a dystrophy of Bowman's layer.

Therapy: Early stages can be compensated with hard contact lenses. Progressed stages require penetrating or deep anterior lamellar keratoplasty.

2.2.3. Herpes simplex virus keratitis

Definition: HSV keratitis is a corneal disorder caused by a primary or a recurrent infection with Herpes simplex virus (HSV 1 or rarely HSV 2)

Epidemiology: 60 % to 95 % of the adult world population is affected by HSV (5). Herpes keratitis results mostly from a reactivation of the virus which has remained in a latent state.

Clinical signs: Holland EJ classified herpes simplex virus keratitis into the following four categories (15): 1. Infectious epithelial keratitis involving corneal vesicles, dendritic ulcers, geographic ulcers, and marginal ulcers. 2. Neurotrophic keratopathy involving punctate epithelial erosions and neurotrophic ulcers. 3. Stromal keratitis involving necrotizing stromal keratitis and immune stromal keratitis. 4. Endotheliitis which can be disciform, diffuse, and linear. Corneal sensation is reduced. Stromal necrotic keratitis is typically represented by a corneal ulcer without hypopyon. It may lead to scarring and/or vascularization (16).

Therapy: Therapy involves topical and systemic antiviral agents as well as topical and systemic steroids in certain cases. Progressed stages (scars or perforation) may require keratoplasty (à chaud).

2.3. The clinical examination of the cornea

The number of corneal examination tools has increased substantially, but there are still limitations in corneal imaging. Slit-lamp biomicroscopy, offering semi-quantitative information on corneal structure, is an essential tool for diagnosis of corneal diseases. In order to obtain more accurate quantitative measurements, ultrasound pachymetry is often required. Its major application in clinical practice consists of the determination of corneal thickness. Endothelial and epithelial measurements can also be achieved by non-contact specular microscopy. Optical Coherence Tomography (OCT) produces cross-sectional views of the cornea. OCT is based on low-coherence interferometry and can be considered analogous to ultrasound imaging, with OCT imaging requiring no direct tissue contact. A broadband light source delivers near-infrared light which reflects off the targeted tissue. The intensity of this reflected light is being measured and computer-processed into a cross-sectional image. Commercially available, the SL – OCT (Heidelberg Engineering, Heidelberg, Germany) allows for simultaneous OCT and slit lamp examinations. It offers an axial optical resolution below 25 μm and a transversal optical resolution below 10 μm . A system for anterior chamber imaging is the Visante™ OCT (Carl Zeiss Meditec AG, Jena, Germany) with a transversal resolution of 60 μm and an axial resolution of 18 μm . High resolution (11) OCT images of the anterior chamber and ultrahigh resolution images (8) with an axial resolution of 2-3 μm have been performed. Wirbelauer (50) reports on clinical experience with Optical Coherence Tomography of the cornea. The corneal epithelium, Bowman's layer, the intrastromal morphology and the endothelium have been visualized in these experiences. The anterior eye segments of patients with a variety of corneal abnormalities have been examined in vivo by high-speed, ultra-high-resolution OCT (6). The only tool available in clinical practice providing views that are parallel to the corneal surface and showing cellular detail is confocal microscopy (29). The HRT Rostock Cornea Module (Heidelberg Engineering, Heidelberg, Germany) offers a transversal resolution of 10 μm and a longitudinal resolution of 62 μm . Applications include the early detection of corneal infection, endothelial cell counting and the description of immune reactions after keratoplasty. The monitoring of corneal wound healing after corneal refractive surgery (9) or observations in long term contact lens wear (26) have been described. Studies using confocal microscopy have been performed in

order to describe corneal anatomy and pathology in vivo more precisely (47). A disadvantage of this method resides in the need for a detection pinhole causing a loss of photons and thus a deterioration of the picture. Furthermore, the short wavelengths used in confocal microscopy cause high light scattering especially in scar tissue and low tissue penetration depth. Objective-cornea contact necessary to perform the images requires high patient compliance and may cause damage to the eye. Disadvantages of this method have been pointed out by Masters and Erie (9, 26). In order to determine corneal disease at an early stage or to monitor its progression, it would be important to obtain morphological and functional information at a subcellular level.

2.4. Refractive surgery: a historical overview

Refractive errors are common. The most frequent eye-sight problem is myopia, with 40% prevalence in the world population. Other errors include hyperopia and astigmatism. Myopia and hyperopia result from an incorrect relation between the eye axis length and the eye refractive power. Astigmatism describes a difference in the degree of refraction in different meridians of the cornea. Refractive glasses, contact lenses and refractive surgery can correct these errors. The first attempts to correct refractive errors took place in the nineteenth century. The dutch physician Jan Lans Leendert tried to flatten the cornea by performing varying incisions. Tsutomu Sato from Tokyo performed a large amount of posterior keratotomies (51). Jose Barraquer introduced lamellar surgery by removing the anterior cornea with a microkeratome, freezing it and changing its shape (51). This was the beginning of keratomileusis. In the 1970's, Russian scientists, mainly Svyatoslav Nikolatevich Fyodorov, refined radial keratotomy (51). Fyodorov determined that a good flattening effect could be achieved with less than 16 incisions placed on the anterior cornea only. He established radial keratotomy in the world. The PERK (Prospective Evaluation of Radial Keratotomy) study supported by the National Eye Institute of the United States was run between 1980 and 1985 in order to provide scientific data on radial keratotomy. Patients treated in a standardized manner were followed up for the next 10 years after the surgery (13, 48). The outcome of the study was that radial keratotomy was safe enough as a procedure, although a gradual hyperopic

shift still existed after 10 years. The ArF excimer laser was first used on blind human eyes by Theo Seiler in 1987. He ablated the corneal surface to cure myopia and introduced photorefractive keratectomy (PRK) (38, 39). In 1990, Ioannis Pallikaris from Crete developed the laser in-situ keratomileusis (LASIK) (33). A corneal flap of approximately 130 μm was being created using a microkeratome and some exposed corneal tissue was being ablated by the excimer laser. Advantages over PRK were the integrity of the epithelium and significantly decreased post-operative pain. Laser subepithelial keratectomy (LASEK) was developed by Dimitri Azar and Massimo Camellin independently (2, 4). In the LASEK procedure, an epithelial flap was being created by a combination of a diluted ethanol solution and a mechanical knife. Stromal tissue was subsequently being ablated by an excimer laser and the flap was being replaced. All procedures included the use of the excimer laser, operating at UV wavelengths (mostly 193 nm).

The biophysical processes involved in UV-light induced photoablation were first discovered by Srinivasan in 1982 when he studied the action of pulsed UV laser radiation on organic polymers (41). UV-light consisted of high energy photons which were absorbed by organic tissue. This caused promotion to repulsive excited states within a molecule leading to dissociation of covalent bonds between atoms. The fragments were being ejected which corresponded to the ablation. An overview of further details on laser-tissue interactions was given by Niemz (32). When comparing dissociation energies of different types of covalent bonds to photon energies of different laser types, it became obvious that only excimer lasers delivered sufficient energy for dissociating such bonds. For the particular excimer laser wavelength of 193 nm, pure photoablation without a thermal component occurred. A drawback of excimer lasers was their low tissue penetration depth, limited to $\pm 5 \mu\text{m}$ due to the high absorption coefficients. This implied that photoablation was only possible in exposed tissue. Deeper tissue layers could be treated only following ablation of superficial tissue. Excimer lasers also included applications outside refractive surgery. They were for instance used in penetrating (40) and in lamellar keratoplasty (24).

In the last years femtosecond lasers have been introduced to refractive surgery. They are currently used for LASIK flap creation, astigmatic keratotomy after keratoplasty, tunnel creation for intrastromal corneal ring segments, lenticule extraction and small incision lenticule extraction, corneal inlays and intrastromal

presbyopia correction (18). Imprecision caused by mechanical microkeratomes account for the highest percentage of intraoperative LASIK complications (25). Flap creation by a femtosecond laser in LASIK allows for greater accuracy in flap creation and thinner flaps (14, 17, 18, 34, 36, 46).

The wavelengths involved in these femtosecond laser systems are within the near-infrared range. Their depth of tissue penetration is relatively high. The used wavelengths are within the optical window of corneal tissue, enabling them to penetrate deeply into tissue while leaving exterior tissue undamaged. Pulse energies are usually low in the range of μJ . Low pulse energies help to reduce damage to surrounding tissue. The principles of tissue removal with amplified femtosecond lasers can be summarized in optical breakdown, formation of cavitation bubbles and shockwave generation, corresponding to photodisruption. These are mechanical effects extending beyond the focus spot and possibly causing undesired damage to the surrounding tissue. They are in a linear relationship with the absorbed energy.

In spite of numerous accomplishments, modern corneal refractive surgery faces a number of challenges. Complications include dry eye syndrome, epithelial defects, lamellar keratitis, haze, epithelial ingrowth, debris, infectious keratitis and ectasia (35).

Most corneal refractive treatments involve the creation of a flap. The idea of intrastromal tissue removal without flap creation appears interesting because certain complications such as flap displacement or lamellar keratitis might become obsolete. Also, since mechanical effects are in a linear relation with the absorbed energy, lower energy laser pulses than those delivered by the amplified femtosecond lasers in use could prove beneficial as they might cause less undesirable damage to the tissue.

2.5. Multiphoton laser scanning microscopy

Two-photon effects were first described by Maria Göppert-Mayer in her doctoral dissertation (12). Two-photon excited fluorescence relies on the ability of a molecule to simultaneously absorb two low energy photons. This quantum event is only likely to occur at light intensities of MW/cm² to GW/cm². In fact, photon fluxes of about 10²³ photons/s/cm² are required. When a molecule absorbs two low energy infra-red photons at one time, it reaches an excited state which would normally require absorption of one high-energy UV photon. Since the relaxation pathway does not depend on the excitation pathway, the results of one-photon and two-photon absorption are similar: the molecule will tend to regain its ground state by emitting fluorescence in the range of visible light (fig. 1). Mean laser powers at the target below 10 mW are sufficient to register autofluorescence in the excited tissue. The physics of a two-photon effect are demonstrated in the Jablonski diagram, which displays molecular states and transitions (fig. 1).

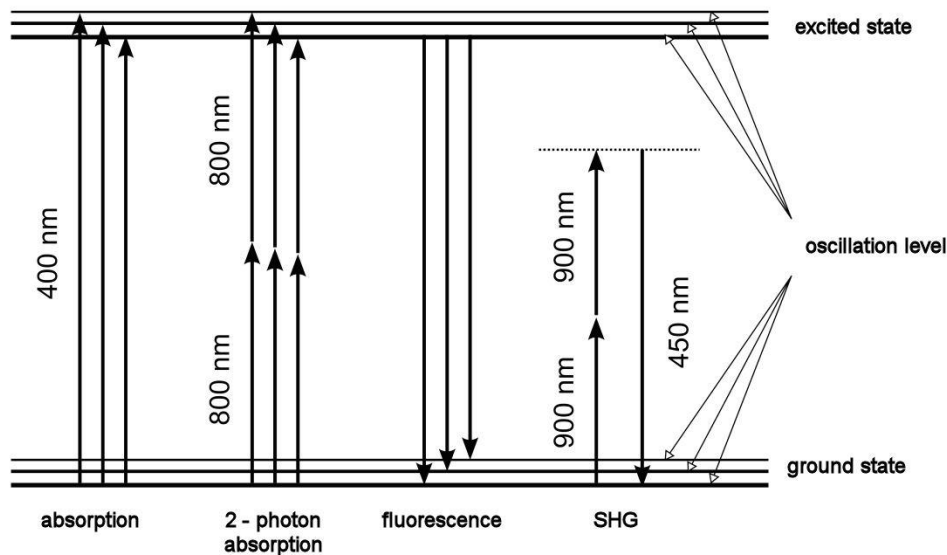


Fig. 1.

The Jablonski diagram displays molecular states and transitions. The energy of each state is shown by its vertical situation. Some typical wavelengths are demonstrated.

One-photon absorption (here 400 nm) and two – photon absorption (here 800 nm) both elevate the molecule to an excited state. In order to regain its ground state, the molecule emits visible light (fluorescence). Shg occurs in asymmetrical molecules. Laser irradiation produces visible light (here 450 nm) at half the incident wavelength (here 900 nm)

Corneal tissue contains endogenous fluorophores such as collagen and the reduced coenzymes NAD(P)H. Their spectral characteristics have been studied (20).

The imaging mode applied in this study relies on such multiphoton effects. As mentioned above, they only occur at peak light intensities. This is a feature offering advantages over confocal laser scanning microscopy. In conventional confocal laser scanning microscopy, *af* arises from within, but also considerably from around the focal plane. In order to improve the image resolution, a detection pinhole is necessary to filter out-of-focus fluorescence. But this also results in a loss of photons, causing a deterioration of the obtained image. In multiphoton microscopy, however, a detection pinhole becomes obsolete, because *af* only arises from where light intensity is high enough, i.e. mainly from within the focal plane. The image quality is thus improved as compared to confocal laser scanning microscopy.

Another multiphoton effect allowing for selective and native tissue imaging is second harmonic generation (shg) (21, 30, 45, 52). Shg is an optical process that occurs in asymmetrical molecules. Laser irradiation of such molecules causes their non-linear polarization and produces light at exactly half the incident wavelength and in the same direction as the incident light (fig. 1).

Af, enabled by multiphoton effects, presents reduced photobleaching and phototoxicity outside the focus. *Af* results from an absorptive, non-linear process.

Shg also results from a non-linear, but not from an absorptive process. Shg therefore causes less photobleaching and phototoxicity. The near-infrared wavelengths involved in both processes offer the advantage of a higher light penetration depth than UV photons. Thick tissues like corneal tissue can easily be imaged at all levels. Both processes do not require staining, but deliver high resolution, real-time images of native tissue.

2.6. Laser-tissue interactions

Laser-tissue interactions have been described by M. Niemz (32). At typical pulse durations of ps to fs and at power densities of 10^{11} - 10^{16} W/cm² as in solid state Titanium-Sapphire lasers, the phenomena of plasma-induced ablation and photodisruption occur during interaction with biological tissue. Laser light intensities of TW/cm² are required to cause an optical breakdown. The applied electric field strength has to be comparable to the intramolecular Coulomb electric field and is the most important parameter for the initiation of plasma formation. The electric field strength E depends on the light intensity I by the basic electrodynamic equation: $I = 1/2 E_0 \times c \times E^2$. During an optical breakdown, photons collide with electrons which accelerate, collide with other atoms and ionize them, thus causing an avalanche of free electrons. The induced plasma expands and can cause photodisruption, consisting in the formation and collapse of cavitation bubbles and shockwave generation. As mentioned above, these undesirable effects of cavitation bubble and shockwave formation are in a linear relationship with the pulse energy. The non-amplified femtosecond laser system applied in this study emitted pulse energies in the nJ range, leading to a decrease in unwanted side-effects.

2.7. Aims of this study

The purpose of this study was to image and cut corneal tissue by means of multiphoton laser scanning microscopy.

Human donor corneas and pathological corneas including Fuchs' endothelial dystrophy, keratoconus and herpes simplex keratitis had to be imaged up to a tissue depth of 200 μ m. The spectrum of emitted signals was analyzed. Optical slicing of the tissue in parallel to its surface was performed (19, 21). Respective advantages of af (autofluorescence) and shg (second harmonic generation) imaging were investigated.

Corneal tissue was cut by increasing laser power at the target. Dependence of lesion width on tissue depth and on pulse energy were determined. Finally, tissue was examined by light microscopy.

3. Materials and Methods

The experiments performed in this study involved porcine and human corneal tissue. Their origin, acquisition and treatment are being described. The corneal tissues were imaged and cut using a femtosecond laser coupled to a laser scanning microscope. Four setups including a mode-locked, non-amplified Titanium-Sapphire femtosecond laser were used.

3.1. Corneal samples

3.1.1. Acquisition and treatment before the laser experiment

3.1.1.1. Porcine corneas

Porcine eye bulbi were enucleated within 2 hours following death of the animal at the abattoir and were stored in cell medium (Gibco[®], D-MEM, high glucose, GlutaMAX[™], Invitrogen GmbH Karlsruhe, Germany) at +4 °C or in saline solution. Corneas were extracted within 8 hrs after the death of the animal using a corneal trephine or corneal scissors and were placed in cell medium at +4 °C for ≤ 1 hour before the start of the experiment. In order to compare state of viability, af and cutting proprieties, some studies were also performed on corneas stored in cell medium for 24-48 hrs or remained in saline solution. Samples were placed in a cell chamber ("MiniCem", JenLab GmbH, Jena, Germany) containing cell medium during the laser microscope experiment.

3.1.1.2. Human corneas

Human pathologic corneal tissue

Progressed stages of certain corneal pathologies such as endothelial dystrophy or keratoconus required keratoplasty. Keratoplasty was a corneal transplantation in which tissue was entirely (penetrating keratoplasty) or partly (lamellar keratoplasty) replaced by the graft. Pathologic corneal tissue extracted either after penetrating or after lamellar keratoplasty was stored in saline solution (Sodium Chloride 0.9 %, B.

BRAUN Melsungen AG, Melsungen, Germany) and processed inside the cell chamber ("MiniCem", JenLab GmbH, Jena, Germany) containing cell medium (Optisol-GS, Bausch & Lomb, Rochester, NY, USA).

Human donor corneas

Human donor corneas were collected in the "Lions Hornhautbank Saar-Lor-Lux, Trier-Westpfalz". After their extraction, donor corneas were placed in a transport solution (Optisol-GS, Bausch & Lomb, Rochester, NY, USA) and stored inside a refrigerator at +4 °C - +8 °C. Maximum storage time was three days until transferral into a different medium (MEM, (Eagle) Liquid Medium, Biochrom AG, Berlin, Germany) and into an incubator at +34 °C. One mL of previously γ -radiated Fetal Bovine Serum (FBS, Biochrom AG, Berlin, Germany) was being added for each cornea. A replacement of the medium was being performed at a weekly rate for a maximum of 4 weeks. An endothelial cell count as well as a bacteriological exam were performed after one week of storage. Transplantation was possible after suitability and sterility of the tissue had been confirmed approximately two weeks after corneal extraction. A suitable cornea was placed into a medium containing additionally 60 g Dextran / 1000 mL one day prior to a planned keratoplasty and could remain here for up to 4 days. If corneas did not comply with the requirements of endothelial cell count, they were excluded from transplantation. Such clinically unsuitable corneas were used in this study. These corneas were otherwise handled in the same way as transplanted corneas. During the experiment, the donor corneas were placed inside the same type of cell chamber as the porcine corneas mentioned above.

3.1.2. Treatment after the laser experiment

Some corneal samples were selected to be analyzed by light microscopy after the laser experiment. In this case, the samples were indulged in fixation medium (Klinik-Fix, 1% glutaraldehyde, 1% formaldehyde in phosphate buffer 0.12 M prepared by the Institute of Anatomy and Cellular Biology, University of Saarland, Homburg/Saar, Germany) immediately after the experiment and placed into a refrigerator. The samples underwent epoxy resin embedding. The embedding procedure started with

washing the samples in phosphate buffer overnight. The samples were osmium-blackened in a 2 % Osmium-solution the next day. Corneas were subsequently fully dehydrated by a series of ethanol solutions of increasing concentration. After dehydration, corneas were placed overnight in an Aceton: Embed (3:1) (Embed12, Electron Microscopy Sciences, Hartfield, PA, USA) solution to be transferred into a series of higher concentration Embed12-solutions the following day. The samples were oriented into their embedding shape and labeled and remained in an incubator at +60 °C for two more days in order to fully polymerize. Light microscopy was performed in order to allow orientation within the corneal tissue. Transversal cuts of a thickness between 0.5 µm and 1 µm were performed using the Reichert Ultracut R (Reichert-Ultracut R, Jung). Samples were then colored in Richardson-solution (Azur II, aqua destillata, methylene blue, borax) prepared by the Institute of Anatomy and Cellular Biology, University of Saarland, Homburg/Saar, Germany and could be viewed by light microscopy.

3.2. System configurations

Mode-locked, non-amplified solid state Titanium-Sapphire lasers (Chameleon™, Coherent Inc., Santa Clara, CA, Mai-Tai™ One Box, Spectra Physics, MountainView, CA, and Vitesse™, Coherent Inc., Santa Clara, CA) were coupled to a laser scanning microscope (LSM510-META™, Zeiss, Jena, Germany).

The Chameleon™ Laser was also coupled to the Dermalnspect™ (JenLab GmbH, Jena, Germany) Tomograph.

Chameleon™ - LSM 510 - META™

A mode-locked, widely tunable, non-amplified solid state Titanium-Sapphire laser (Chameleon™, Coherent Inc., Santa Clara, CA) was coupled to a laser scanning microscope (LSM510-META™, Zeiss, Jena, Germany). The laser had a tuning range of 720 - 930 nm and a repetition rate of 90 MHz. The maximum output power was 1 W, corresponding to 11.1 nJ pulse energy. Pulse width was between 136 fs and 170 fs at the output and between 276 fs and 335 fs at the target due to optical dispersion effects. Pulse widths were measured using an autocorrelator ("Mini", APE GmbH, Berlin, Germany).

Mai Tai™ One Box - LSM 510 - META™

A Titanium - Sapphire laser (Mai Tai™ One Box, Spectra Physics, Mountain View, CA) was coupled to the LSM 510™. Although the laser had a wide tuning range all corneal cuttings were performed at $\lambda = 800$ nm. The repetition rate was 80 MHz. The maximum output power was 2.5 W. The pulse width was 100 fs at the output.

Vitesse™ - LSM 510 - META™

A Titanium - Sapphire laser (Vitesse™, Coherent Inc., Santa Clara, CA) was coupled to the laser scanning microscope (LSM 510 - META™, Zeiss, Jena, Germany). The laser had a set wavelength of 800 nm and a repetition rate of 80 MHz. The maximum output power was 650 mW, corresponding to a pulse energy of 8.1 nJ. The pulse width was 100 fs at the output.

Chameleon™ - DermalInspect Tomograph™

The Chameleon™ laser was coupled to the DermalInspect™ (JenLab GmbH, Jena, Germany) Tomograph (20). The laser was coupled to a scanning module with a fast x,y galvanometer, piezodriven 40x focusing optics with a high NA of 1.3 (oil) and 200 μm working distance. A fast PMT detector module as well as a control unit including JenLab Image software for processing was used. The set-up was used to acquire images of human donor corneas in the af and in the shg mode.

The laser beam was focused through a 40 x oil-immersion objective (ZeissNeofluar™, Zeiss, Jena, Germany) with a numerical aperture of 1.3 in each configuration. A short-pass filter KP650 in front of the photomultiplier prevented detection of backscattered laser light. Powers at the target were between 5 and 20 mW for imaging and up to 200 mW for cutting. This corresponded respectively to pulse energies of 2.2 nJ for the Chameleon and 2.5 nJ for the Vitesse™ and Mai Tai™ One Box. The laser power at the objective was determined before each experiment by means of a power meter (FieldMaster™, Coherent Inc., Santa Clara, Ca, USA).

The sample was placed inside a cell chamber ("MiniCem", JenLab GmbH, Jena, Germany) located on a micropositioning table. Corneal epithelium was facing the laser beam. Images in the horizontal (x; y) plane were obtained and viewed in a frame consisting of 512 pixels x 512 pixels corresponding to 230 μm x 230 μm , unless otherwise specified. A z-motor allowed moving the sample vertically. In order to determine the most superficial cellular layer, an automated contrast finder was applied and the z-level was manually adjusted. The superficial plane was set to a z-

position = 0. The z-motor allowed for 1 μm steps with a maximum tissue penetration depth of 200 μm . This limitation was due to the working distance with a high numeric aperture objective. To perform corneal tissue processing, a line scanning function was used. The laser beam was parked on a horizontal line consisting of 1 x 512 pixels. A scanning time of 15 s was used for most cuttings. This scanning time corresponded to a pixel dwell time of 977 μs .

3.3. Choice of scanning time

Two porcine corneas stored in cell medium for 3 respectively 5 hrs before the experiment were imaged. The laser wavelength was 800 nm. The purpose was to determine a scanning time for studies on lesion width - pulse energy and lesion width – tissue depth dependence. Lesion width increased in both corneas as the pixel dwell time increased to 977 μs corresponding to a scanning time of 15 s. Fig. 2 and 3 show the lesion widths in relation of the scanning times in the two corneas. A scanning time of 15 s was maintained for the following experiments.

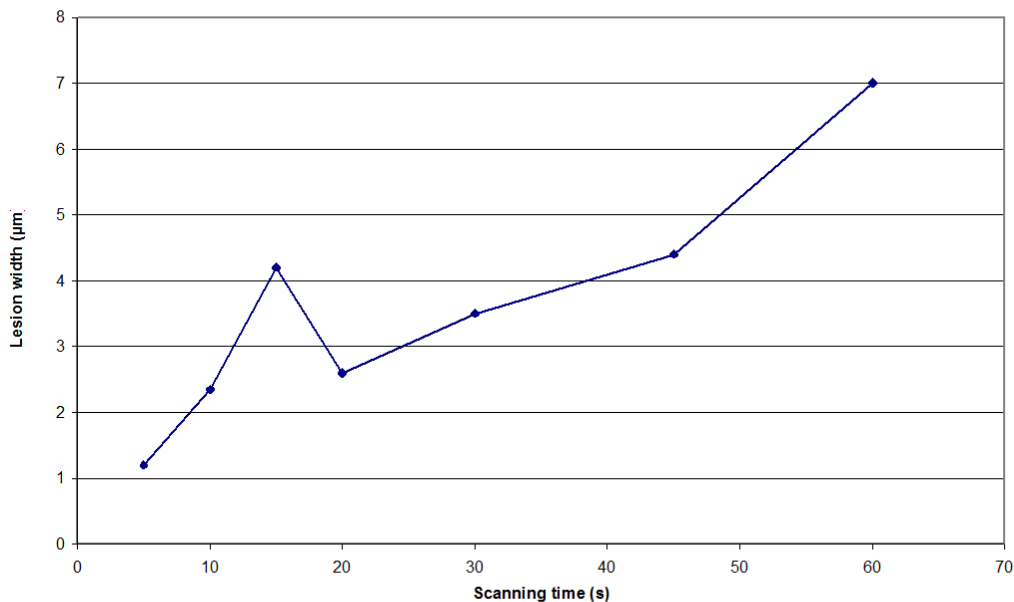


Fig. 2

Lesion width depending on scanning time. The horizontal axis displayed the scanning time in seconds, the vertical axis the lesion width in μm . Lesions were

created using the Mai-Tai™ One Box coupled to the LSM510-META™ in porcine cornea. Plasma luminescence was measured in 3 defined localizations determined by the superposition of a grid.

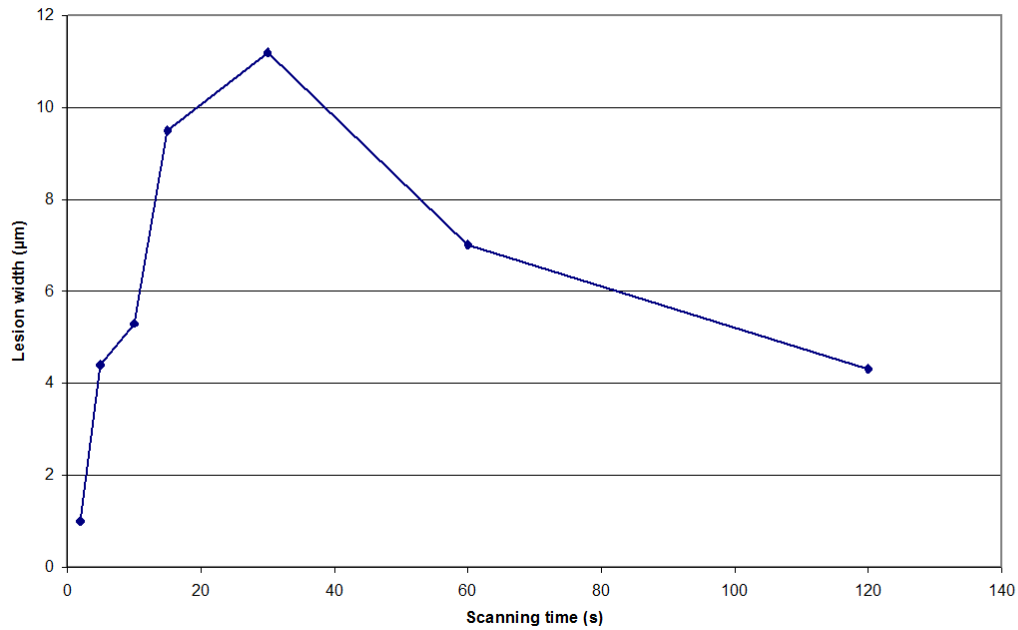


Fig. 3

Lesion width depending on scanning time. The horizontal axis displayed the scanning time in seconds, the vertical axis the lesion width in µm.

Lesions were created using the Chameleon™ coupled to the LSM510-META™ in porcine cornea. Plasma luminescence was measured in 3 defined localizations determined by superposition of a grid.

4.1.1. Epithelium

Excitation at 740 nm and at 800 nm revealed a detailed morphologic description of corneal epithelium. At 740 nm, corneal cells appeared delimited by a dark cell membrane and contained a dark nucleus. Cytoplasm was brightly fluorescent. Changes in epithelial cell morphology were observed with increasing tissue depth. Corneal apical cells appeared wide and flat (fig. 4). Wing cells were smaller, polygonal, with a very large nucleus compared to the cytoplasm and contained less mitochondria (fig. 6). Basal cells were elongated, with a large ovoid nucleus (fig. 8). At 800 nm, epithelial cells had a dark nucleus and membrane. Cell cytoplasm showed less contrast with nuclei and cell membranes (fig. 5, 7, 9). Cell shapes and the different cell layers could still be identified. The upper layers of apical cells were recognizable as wide and flat (fig. 5). The smaller, polygonal shape of wing cells (fig. 7) and the elongated shape of basal cells (fig. 9) were also noticeable.

4.1.2. Stroma

4.1.2.1. Autofluorescence

Excitation at 760 nm showed a bright keratocyte cell cytoplasm and branches (fig. 10). Keratocytes presented a star-shaped body with a large nucleus and branches forming a communicating network. This cellular network became denser with increasing tissue depth. A discrimination of the collagen matrix was not possible at this excitation wavelength.

4.1.2.2. Second harmonic generation

At an excitation wavelength of 800 nm, the spatial organization of collagen lamellae was revealed. Lamellae were mainly organized in a parallel pattern. Cellular structures such as keratocytes were not identified (fig. 11).

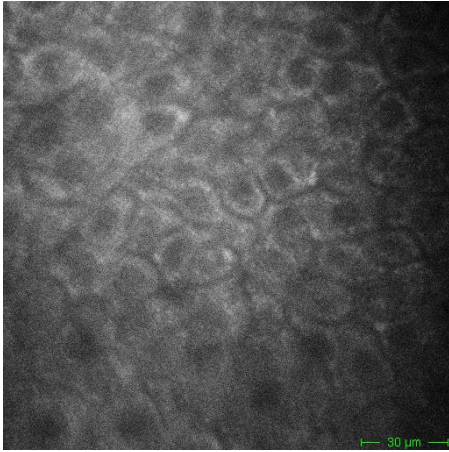


Fig. 4

Af image of the epithelium of a human donor cornea showing apical cells with a dark membrane and nucleus. Cells appeared broad and flat. Tissue depth was 10 μm , the excitation wavelength was 740 nm. The Chameleon™ laser was coupled to the Dermalnspect™ Tomograph.

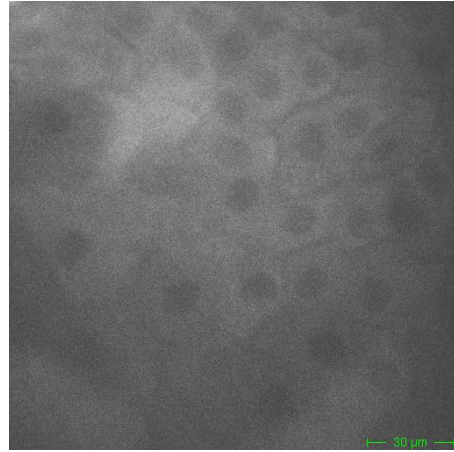


Fig. 5

Af image of the epithelium of a human donor cornea showing apical cells. Cells were large and flat. Cell nuclei and membranes are dark, but paler than at an excitation wavelength of 740 nm. The the first cell layer was imaged, the excitation wavelength was 800 nm. The Chameleon™ laser was coupled to the Dermalnspect™ Tomograph.

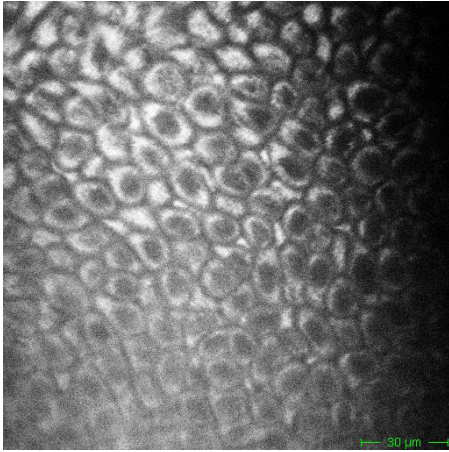


Fig. 6

Af image of the epithelium of a human donor cornea showing wing cells. Cells were smaller, more polygonal and contained a large nucleus. Cytoplasm contained less mitochondria. Tissue depth was 20 μm , the excitation wavelength was 740 nm. The Chameleon™ laser was coupled to the Dermalnspect™ Tomograph.

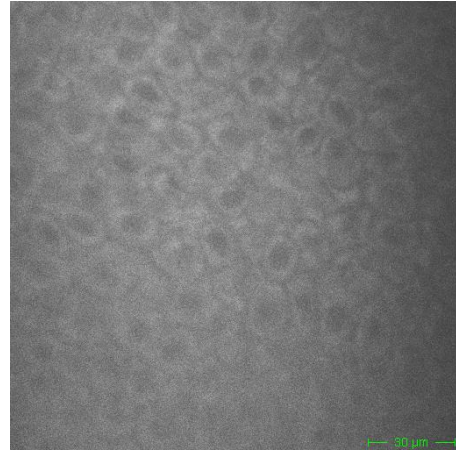


Fig. 7

Af image of the epithelium of a human donor cornea showing wing cells at a tissue depth of 20 μm . The excitation wavelength was 800 nm, Cells could not be discriminated as well as with an excitation wavelength of 740 nm. The Chameleon™ laser was coupled to the Dermalnspect™ Tomograph.

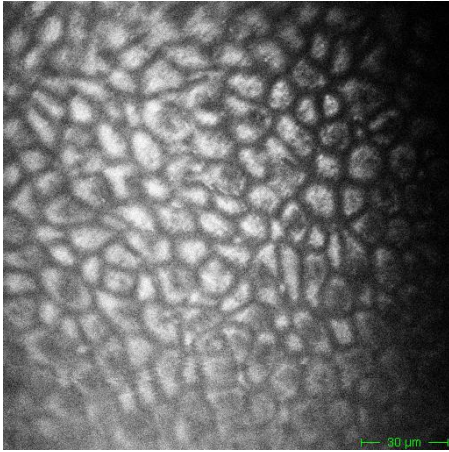


Fig. 8

Af image of the epithelium of a human donor cornea showing basal cells. Cells were polygonal and elongated with a relatively large nucleus. Tissue depth was 40 μm , the excitation wavelength was 740 nm. The Chameleon™ laser was coupled to the DermalInspect™ Tomograph.

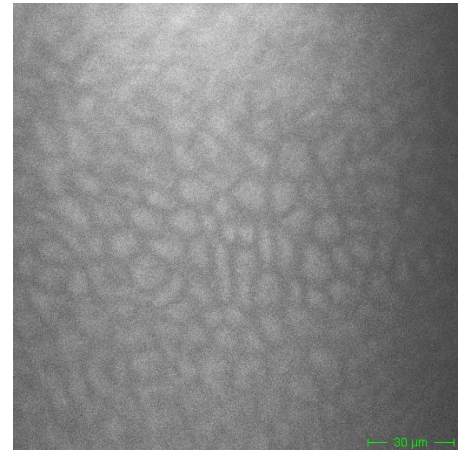


Fig. 9

Af image of the epithelium of a human donor cornea showing basal cells at 40 μm . The excitation wavelength was 800 nm. The Chameleon™ laser was coupled to the DermalInspect™ Tomograph.

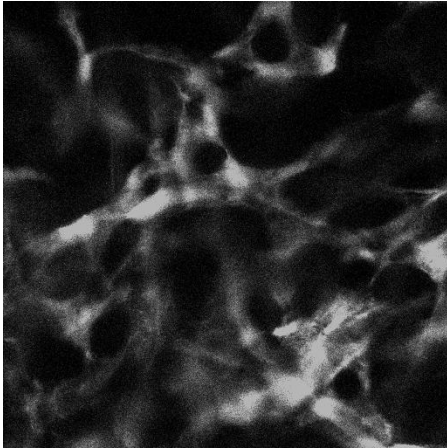


Fig. 10

Af image of the stroma of a human cornea. The keratocyte network and the dark nuclei were well visible. The excitation wavelength was 760 nm, tissue depth was 150 μm . The ChameleonTM laser was coupled to the LSM510-METATM.

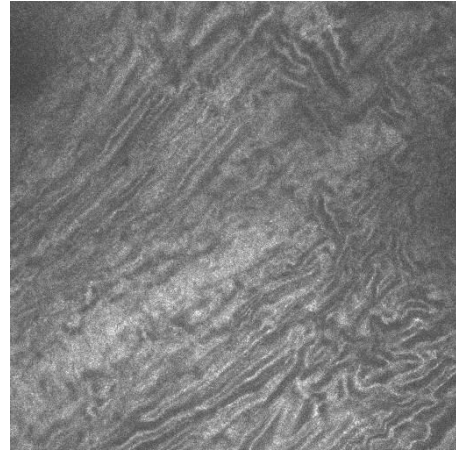


Fig. 11

Shg image of the stroma of a porcine cornea displaying collagen lamellae. Cellular components did not appear. Tissue depth was 80 μm , the excitation wavelength was 800 nm. The ChameleonTM laser was coupled to the DermalInspectTM Tomograph.

4.1.2.3. Morphological intrastromal observations

The stroma of a human donor cornea stored for 26 days was compared to the stroma of a human donor cornea stored for 46 hrs. Examined stromal depths were comparable and conservation media identical. Af and shg images were performed. Af images did not reveal stromal cellular details. In the sample stored for 46 hrs, a small amount of af exposed keratocyte fragments. In the sample stored for 26 days there were no cellular details. However, fluorescent filamentous structures were visible here (fig. 12).

Shg images displayed collagen lamellae in both samples. In the sample stored for 26 days the filamentous structures visible in af imaging could also be observed in shg. In the sample stored for 46 hrs, the SHG mode revealed collagen lamellae only without any cellular or filamentous structures.

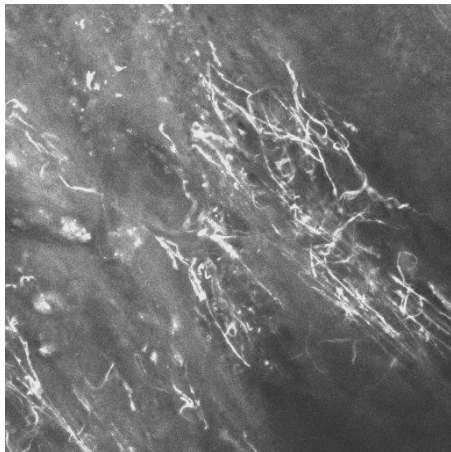


Fig. 12

Af image of the peripheral stroma of a human donor cornea. Keratocytes were not visible, but fluorescent filamentous structured became apparent. Tissue depth was 60 μm , the excitation wavelength was 750 nm. The donor cornea had been stored in cell medium for 26 days. The Chameleon™ laser was coupled to the LSM510-META™.

4.2. Imaging pathologic human corneas

4.2.1. Keratoconus

To obtain images of the epithelial cell layers at high resolution, Af imaging at an excitation wavelength of 740 nm was chosen (fig. 13, 14, 15). Stroma was imaged at excitation wavelengths of 740 nm and 820 nm respectively. Two distant areas within the central cornea were examined in order to avoid artifacts. Laser scanning microscopy revealed a regular appearance of epithelial cell layers. Apical, wing and basal cells were distinguishable. Fig. 13 showed the large and flat apical cells, fig. 14 showed smaller, polygonal cells with a relatively large nucleus and fig. 15 showed elongated, polygonal basal cells. The basal epithelial cell layer appeared interrupted by acellular, most likely collagenous tissue (fig. 16). Immediately below this level, collagenous tissue containing brightly fluorescent dot-shaped deposits became visible (fig. 17). The amount of the deposits decreased with increasing tissue depth. At a tissue depth of 90 μm , very few deposits remained (fig. 18). Both af and shg imaging revealed the deposits. Overall the thickness of the epithelium was reduced in this sample as compared to the normal epithelial thickness of approximately 50 μm .

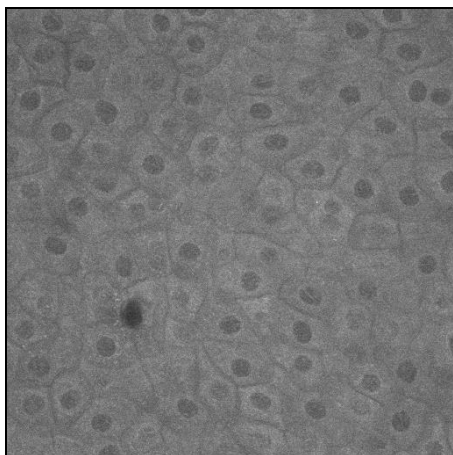


Fig. 13

Af image of the epithelium of a cornea diagnosed with keratoconus. Apical cells were visible at $z = 0 \mu\text{m}$. Dark nuclei and membranes contrasted with the lighter cytoplasm. The excitation wavelength was 740 nm. The Chameleon™ laser was coupled to the LSM510-META™.

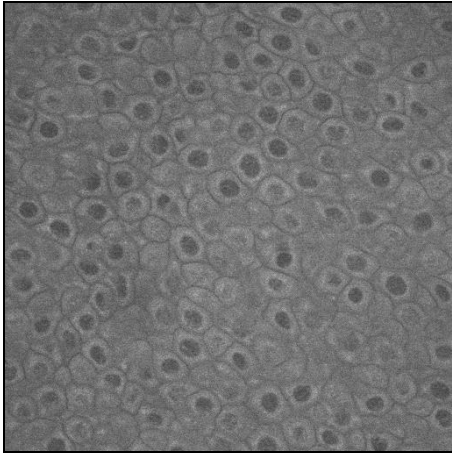


Fig. 14

Af image of the epithelium of a cornea diagnosed with keratoconus.

Smaller wing cells with a relatively large dark nucleus and membrane were visible.

Tissue depth was 10 μm , excitation wavelength was 740 nm. The Chameleon™ laser was coupled to the LSM510-META™.

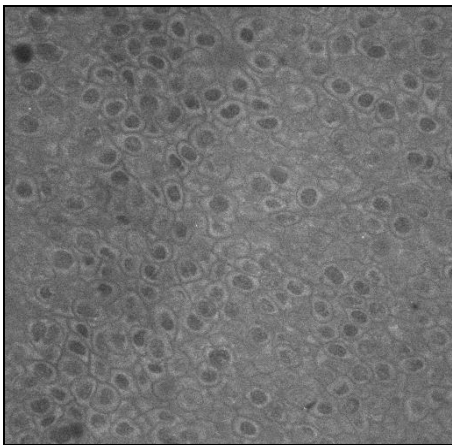


Fig.15

Af image of the epithelium of a cornea diagnosed with keratoconus at a tissue depth

of 20 μm . Polygonal cells with relatively large nuclei were visible. The excitation

wavelength was 740 nm. The Chameleon™ laser was coupled to the LSM 510-META™.

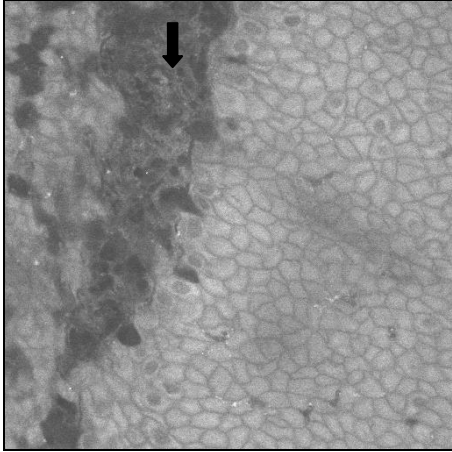


Fig. 16

Af image of the epithelium of a cornea diagnosed with keratoconus. Polygonal and elongated cells are visible. The cell layer was interrupted by acellular tissue (arrow). Tissue depth was 30 μm , the excitation wavelength was 740 nm. The Chameleon™ laser was coupled to the LSM510-META™.

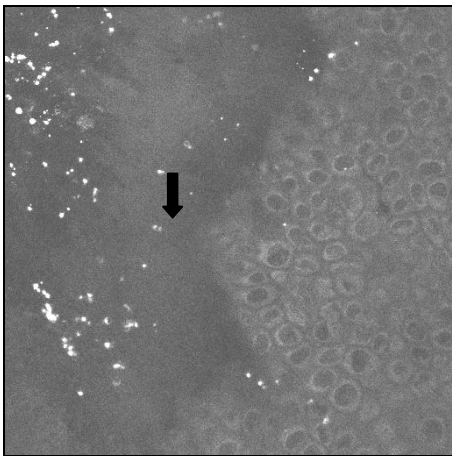


Fig. 17

Af image of the epithelium of a cornea diagnosed with keratoconus. Cellular tissue consisting of polygonal cells was invaded by acellular tissue (arrow) containing highly luminescent particles. Tissue depth was 30 μm an excitation wavelength was 740 nm. The Chameleon™ laser was coupled to the LSM 510-META™.

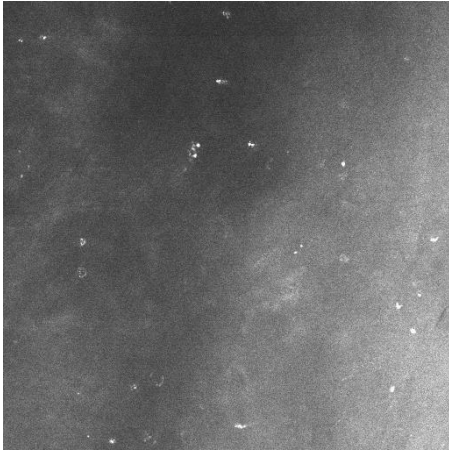


Fig. 18

Af image within the stroma of a cornea diagnosed with keratoconus.

Some luminescent particles appeared. No cellular or collagen structures were visible. The tissue depth was 90 μm and excitation wavelength was 740 nm. The Chameleon™ laser was coupled to the LSM510-META™.

A spectral analysis was performed in order to describe the spectrum of emitted wavelengths in selected intrastromal areas depending on the excitation wavelength. Excitation wavelengths of 800 nm and of 860 nm were applied in selected tissue areas. Emitted signal intensity and spectrum from each region of interest (ROI) were registered for each excitation wavelength (fig. 19 and 20). Emitted signals were registered in a range between 400 nm and 700 nm. Higher emitted wavelengths were excluded in order to avoid confusion with the excitation wavelengths.

Fig. 19 shows the emittance spectrum of selected areas in the superficial stroma of a cornea diagnosed with keratoconus. Luminescent intrastromal areas were marked by ROI 1, 2, 4 and 5. The dark “background” was marked by ROI 3.

The emittance spectrum of ROI 3 showed a peak at 400 nm with little signal in other wavelengths. The emittance spectrum of the luminescent particles also showed a peak at 400 nm. The intensity of this peak was lower than in the background signal with a higher diffuse signal recorded covering the range of other wavelengths.

Similar results were obtained with an excitation wavelength of 860 nm (fig. 20). The dark background signal here was represented by ROI 1. An intensity peak appeared for a wavelength of 430 nm. Some diffuse signals persisted for all other

wavelengths. The luminescent spots emitted a weaker maximum at 430 nm, with a more intense diffuse signal for other wavelengths.

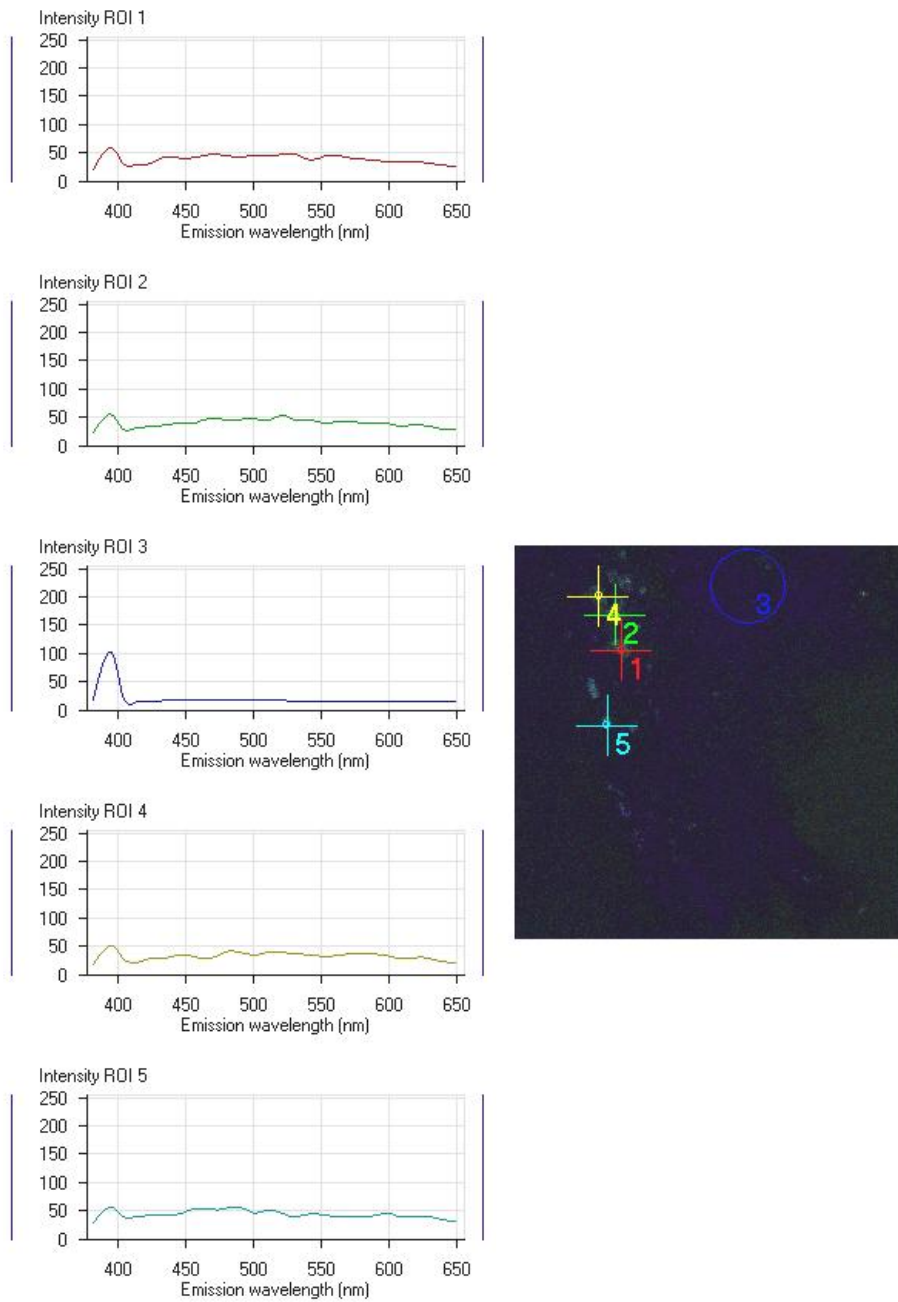


Fig. 19

Superficial stroma of a cornea diagnosed with keratoconus.

Tissue depth was 30 μm and excitation wavelength was 800 nm.

The background signal was marked by ROI 3 (dark blue circle). ROI's 1, 2, 4 and 5 (yellow, green, red and blue targets) mark luminescent areas. The background signal (ROI 3) shows an emitted intensity maximum at 400 nm with very weak signals in the range of 400 nm – 650 nm. The luminescent areas show a weaker intensity maximum at 400 nm and a diffuse signal throughout the registration range. The Chameleon™ laser was coupled to the LSM510-META™.

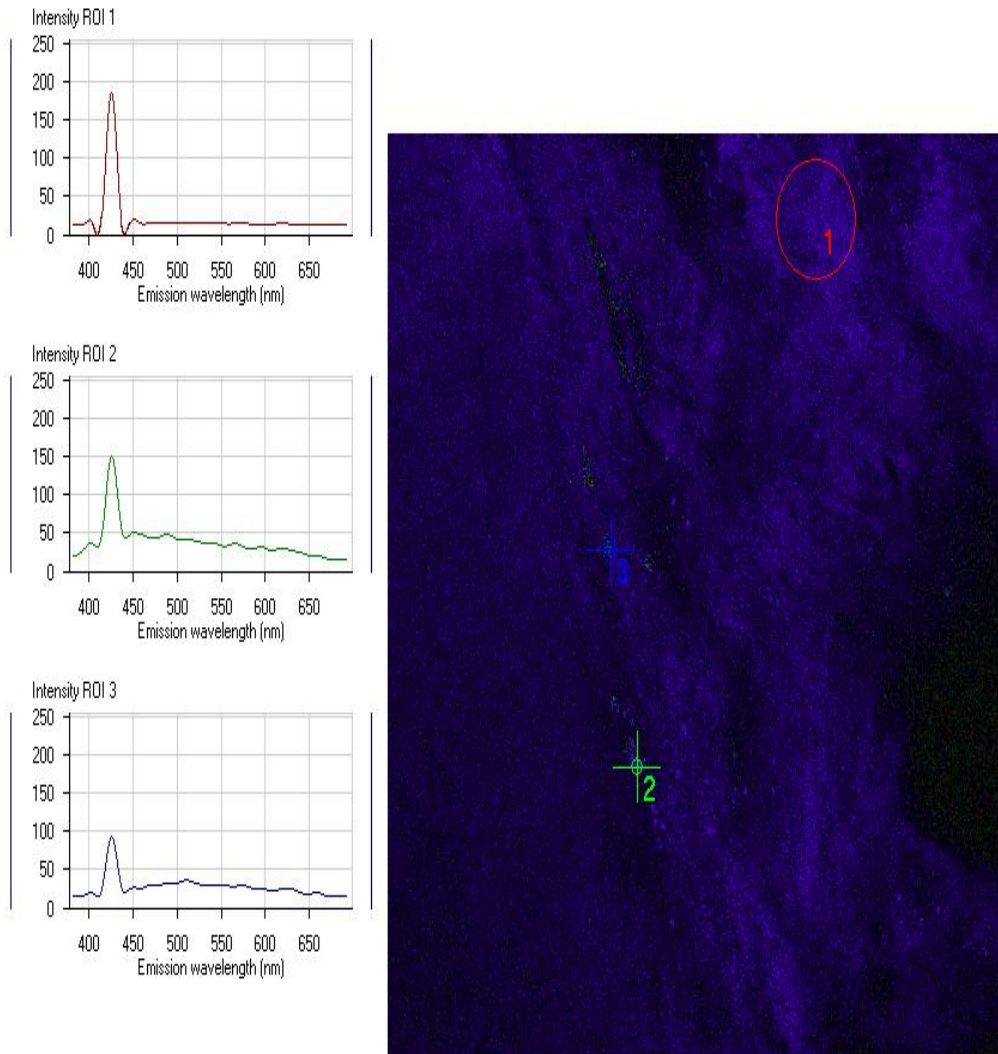


Fig. 20

Superficial stroma of a cornea diagnosed with keratoconus.

Tissue depth was 30 μm and excitation wavelength was 860 nm.

The background signal was represented by ROI 1 (red circle): one peak occurred at

430 μm and almost no other background signal. Luminescent regions were represented by ROI's 2 and 3 (green and blue target): a weaker peak at 430 μm and a diffuse background signal occurred throughout the registration range. The Chameleon™ laser was coupled to the LSM510-META™.

4.2.2. Fuchs' endothelial dystrophy

Corneal tissue diagnosed with Fuchs' endothelial dystrophy was examined using the Chameleon™ coupled to the LSM510-META™ (fig. 21 – 27). Unlike in normal cornea superficial layers of large, flat wing cells could not be identified. Cells appeared small, round and irregular. The aspect of pathologic epithelium imaged in af differed from normal corneal epithelium, as cell constituents were not clearly distinguishable (fig. 21). The nucleus did not appear significantly darker than the cytoplasm. Certain areas within the epithelium, mostly circular, lacked any autofluorescent or luminescent elements. At $z = 35 \mu\text{m}$, linear structures reaching into the epithelium became apparent (fig. 22). No parallel organization of collagen fibrils was visible in shg imaging. A network of keratocytes, imaged in af, became denser with increasing tissue depth (fig. 23, 24 and 25, 26). The corneal endothelium was imaged in LSM while the posterior lamellae were facing the microscope objective (fig. 27). This was necessary because of the objective's limited working distance of 200 μm . Cell limitations were visible so that an endothelial cell count could be performed. Unlike in epithelial cells, cell nuclei could not be discriminated in each endothelial cell. Cell limitations were darker than cytoplasm and thus marked the border of each cell. 1360 cells / mm^2 were counted. Guttae could not be visualized in the LSM images, but were visible in light microscopy (fig. 28).

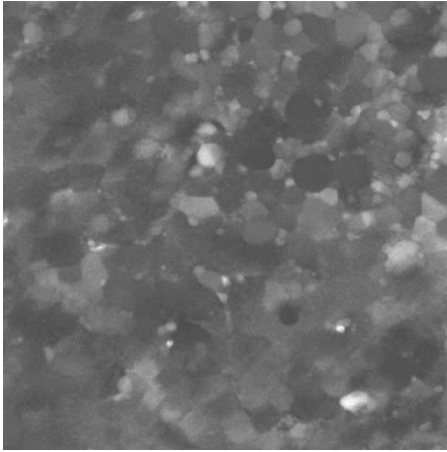


Fig. 21

Af image of the epithelium of a cornea diagnosed with Fuchs' endothelial dystrophy and imaged 46 hrs after penetrating keratoplasty. At a tissue depth of 10 μm and at an excitation wavelength of 750 nm, round luminescent structures and round areas lacking any luminescent elements could be distinguished. Nuclei and cell membranes were not visible. The Chameleon™ laser was coupled to the LSM510-META™.

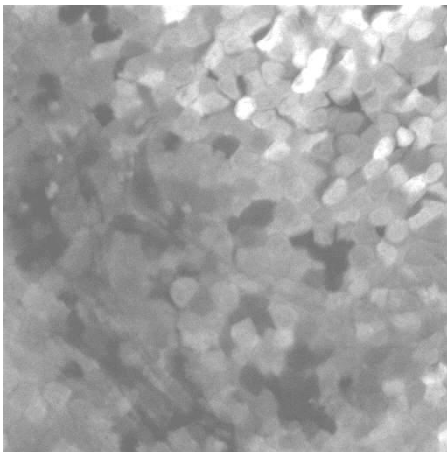


Fig. 22

Af image of the epithelium of a cornea diagnosed with Fuchs' endothelial dystrophy at $z = 35 \mu\text{m}$ and at an excitation wavelength of 750 nm, imaged 46 hrs after penetrating keratoplasty. Nuclei and cell membranes were not visible. Dark linear structures reaching into the epithelium appeared. The Chameleon™ laser was coupled to the LSM510-META™.

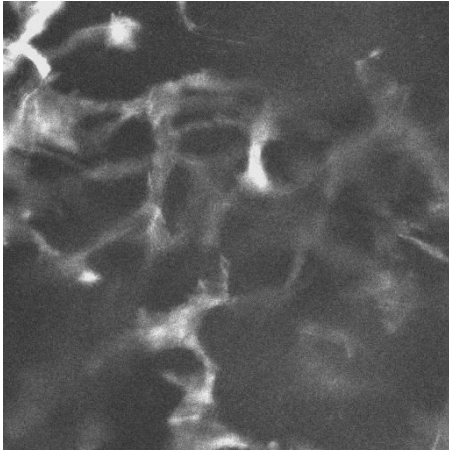


Fig. 23

Af image of the stroma of a cornea diagnosed with Fuchs' endothelial dystrophy, examined 46 hours after penetrating keratoplasty. Tissue depth was 85 μm , the excitation wavelength was 750 nm. A network of keratocyte branches became visible. The Chameleon™ laser was coupled to the LSM510-META™.

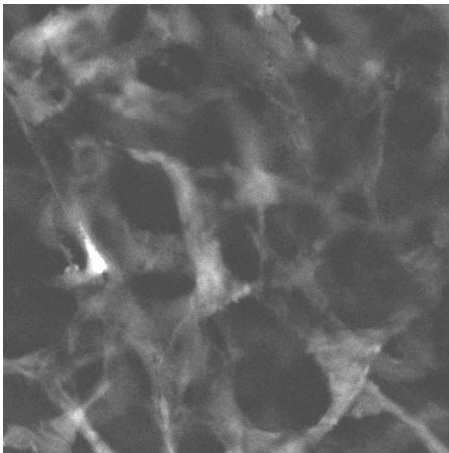


Fig. 24

Af image of the stroma of a cornea diagnosed with Fuchs' endothelial dystrophy, examined 46 hours after penetrating keratoplasty. Tissue depth was 180 μm , the excitation wavelength was 750 nm. The keratocyte network was well visible and denser than at $z = 85 \mu\text{m}$. The Chameleon™ laser was coupled to the LSM510-META.

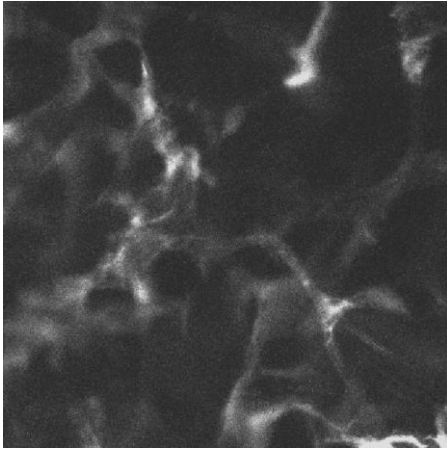


Fig. 25

Af image in the stroma of a cornea diagnosed with Fuchs' endothelial dystrophy examined 24 hrs after penetrating keratoplasty. The keratocyte network appeared. Tissue depth was 125 μm , the excitation wavelength was 750 nm. The Chameleon™ laser was coupled to the LSM510-META™.

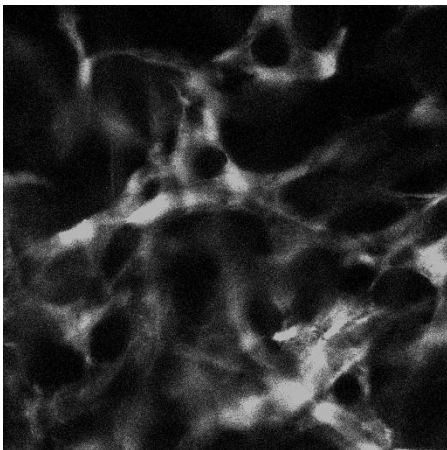


Fig. 26

Af image of the stroma of a cornea diagnosed with Fuchs' endothelial dystrophy examined 24 hrs after penetrating keratoplasty. Tissue depth was 159 μm , the excitation wavelength was 750 nm. A denser keratocyte network as compared to fig. 26 appeared. The Chameleon™ laser was coupled to the LSM510-META™.

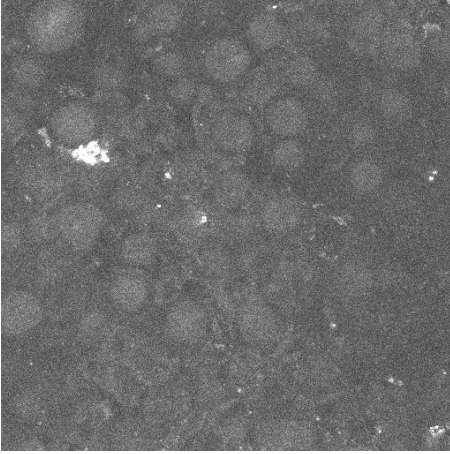


Fig. 27

Af image of the endothelium of a cornea diagnosed with Fuchs' endothelial dystrophy examined 24 hrs after penetrating keratoplasty. The sample was examined with the endothelium facing the objective. Tissue depth was 2 μm and the excitation wavelength was 750 nm. The Chameleon™ laser was coupled to the LSM 510-META™.

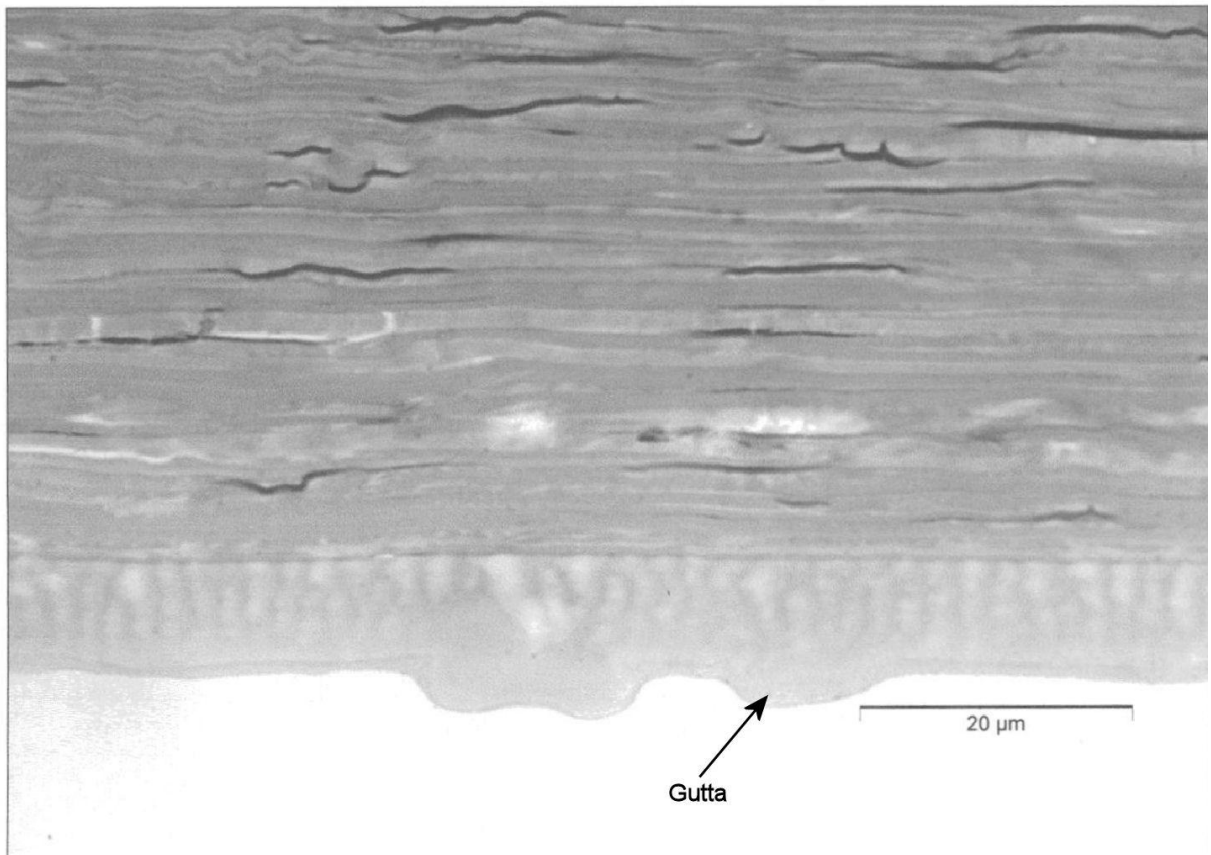


Fig. 28

Light microscopy of the cornea diagnosed with Fuchs' endothelial dystrophy subjected to imaging in fig. 25 – 27.

The endothelium, Descemet's membrane and the posterior lamellae of the stroma were visible. The endothelium included irregularities most likely corresponding to guttae.

4.2.3. Herpes simplex virus keratitis

A human cornea extracted during lamellar keratoplasty was imaged one hour later using the Chameleon™ laser coupled to the LSM510-META™ (fig. 29 – 31). The obtained images suggested a decreased epithelial thickness. The regular order of epithelial cell layers including apical, wing and basal cells could not be identified. In the outermost plane of apical cells smaller wing cells were already found, suggesting irregularity in the composition of the cell layers (fig. 29). Furthermore, the epithelium was invaded by acellular tissue in a depth between $z = 5 \mu\text{m}$ to $z = 30 \mu\text{m}$ (fig. 29 - 31). Light microscopy indicated that this tissue might have represented an enlarged basal membrane. Imaging in two distant areas within the same sample confirmed the findings. Light microscopy (fig. 32) of this specimen revealed a thin epithelium of less than $20 \mu\text{m}$. The epithelial surface was smooth, however cells were flat and enlarged. The basal membrane appeared to be dense.

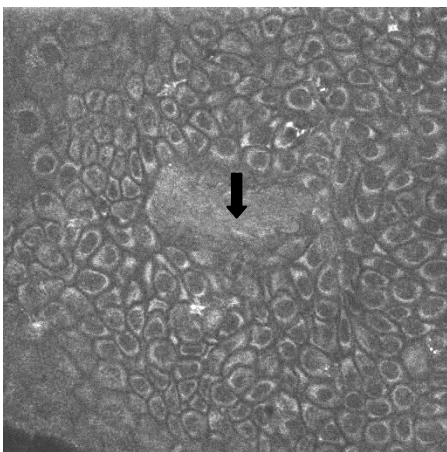


Fig. 29

Af image of the epithelium of a cornea diagnosed with herpes simplex virus keratitis. Tissue depth was $15 \mu\text{m}$, excitation wavelength was 750 nm . Flat cells resembling apical cells appeared as well as smaller, polygonal cells. In the center of the picture

acellular tissue became visible (arrow). The Chameleon™ laser was coupled to the LSM 510-META™.



Fig. 30

Af image of the epithelium of a cornea diagnosed with herpes simplex virus keratitis. Tissue depth was 5 μm , the excitation wavelength was 750 nm. Acelluar tissue invaded epithelial, apical cells (arrow). The Chameleon™ laser was coupled to the LSM510-META™.

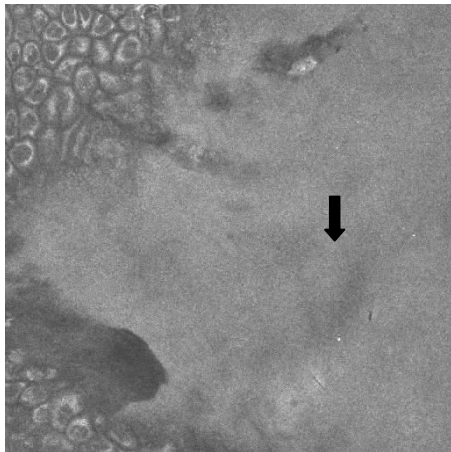


Fig. 31

Af image of the epithelium of a cornea diagnosed with herpes simplex virus keratitis. Tissue depth was 30 μm , the excitation wavelength was 750 nm. Some polygonal cells were visible next to acellular tissue (arrow). The Chameleon™ laser was coupled to the LSM510-META™

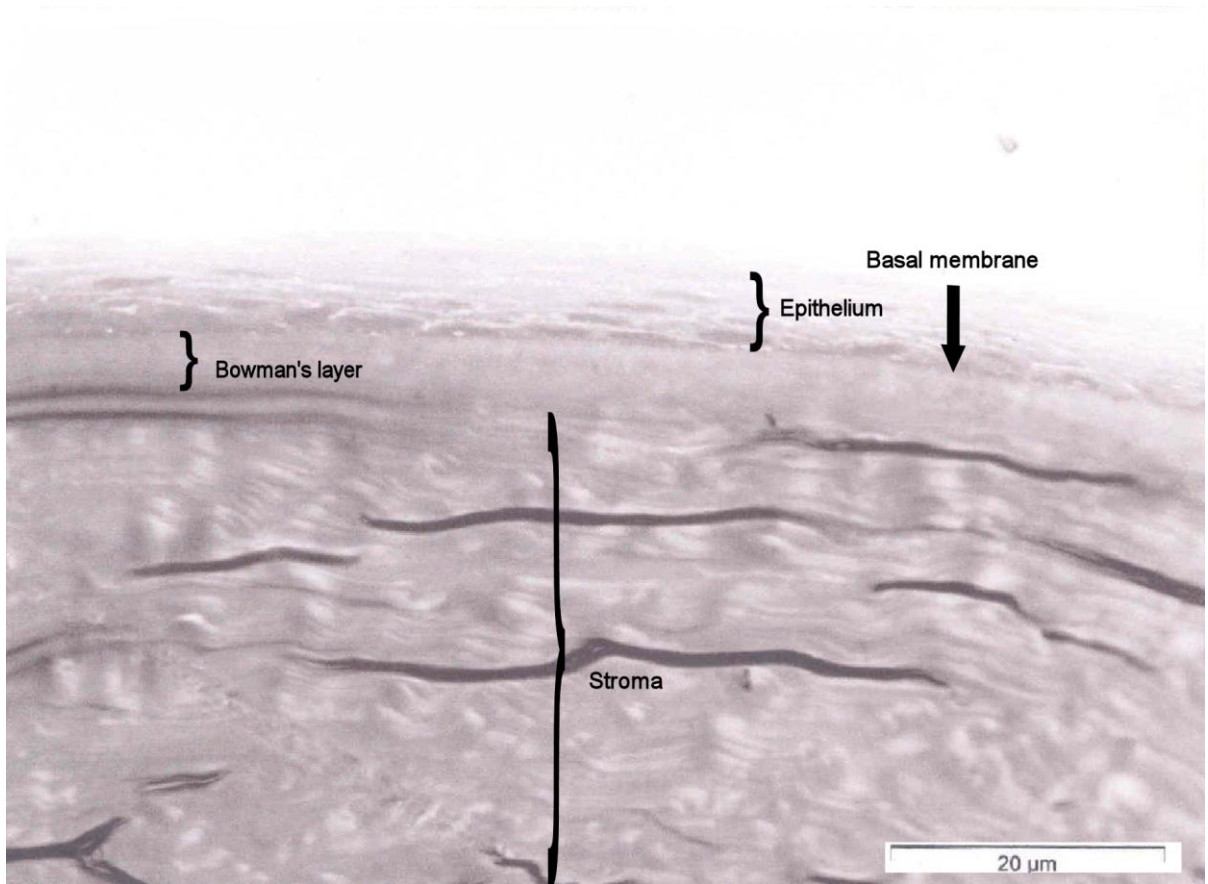


Fig. 32

Light microscopy of the epithelium, basal membrane, Bowman's layer and stroma of a cornea diagnosed with herpes simplex virus keratitis, examined in laser scanning microscopy one hour after lamellar keratoplasty.

4.3. Cutting of corneal tissue

4.3.1. Morphology

Intrastromal linear tissue ablation was performed in four different corneal tissues using identical scanning properties with the Chameleon™ laser coupled to the LSM510-META™. The purpose of this experience was to describe and compare the morphology of intrastromal linear cutting in porcine and human corneal tissues in a recently extracted sample and in an older sample (fig. 33 - 36). The porcine samples were prepared ≤ 8 hrs or 48 hrs before the laser experiment. The human corneal samples consisted of a cornea diagnosed with keratoconus gained 2 hrs before the experiment and of a cornea diagnosed with Fuchs' endothelial dystrophy gained 46 hrs before the laser experiment. Each corneal sample was placed in saline solution (Sodium Chloride 0.9 %, B. BRAUN Melsungen AG, Melsungen, Germany) immediately after its extraction and during the experiment.

For each cornea, three line scans were performed at a tissue depth of $z = 70 \mu\text{m}$. This level was intrastromal for each cornea. The outermost epithelial cell layer corresponded to $z = 0$. The laser power at the output was 100 mW corresponding to a pulse energy of 1.1 nJ. The first line scan was performed at $\lambda = 720 \text{ nm}$, the second at $\lambda = 760 \text{ nm}$, the third at $\lambda = 800 \text{ nm}$. Fig. 33 showed the linear scans within the fresh porcine cornea and fig. 34 showed the linear scans within the aged porcine cornea. Fig. 35 showed the human sample obtained after 2 hrs and fig. 37 showed the human corneal sample obtained after 46 hrs. A highly luminescent plasma along the scanning line indicated the laser-tissue interaction in fig. 33. The plasma had a variable width along the scanning lines. In the third line scan in fig. 33, the plasma was discontinued and was replaced over a short distance by a thin line lacking any fluorescent or luminescent elements and thus appearing as a black line. The luminescent plasma visible in this image resulted from the optical breakdown caused by the high laser light intensities applied along the scanning line. Fig. 34 showed linear tissue ablation performed in a porcine cornea extracted 48 hrs earlier. The plasma luminescence described in fig. 33 was reduced. Instead, the laser-tissue interaction was mainly indicated by a fine and regular appearing black line lacking fluorescent and luminescent elements. The first line scan still included some luminescent elements close to the scanning line. In fig. 35 and 36, laser-tissue

interactions were indicated by a thin, black line showing no irregularities. Fig. 35 showed linear scans within the stroma of a cornea extracted 2 hrs earlier and fig. 36 showed linear scans within the stroma of a cornea extracted 46 hrs earlier.

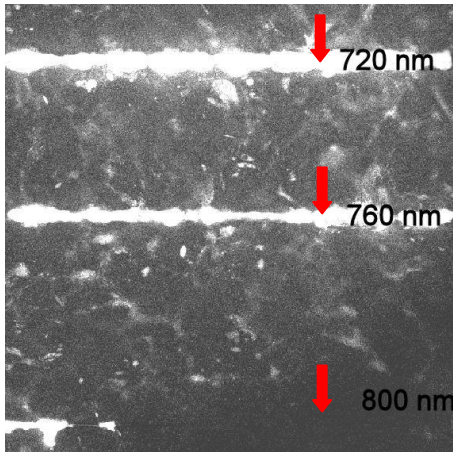


Fig. 33

Linear scans in a porcine cornea, performed 2 hrs after extraction. Excitation wavelengths for each line scan are indicated. Tissue depth was 70 μm .

A luminescent line of variable width appeared in the scanning area. The Chameleon™ laser was coupled to the LSM510-META™. At 800 nm, only few luminescences could be detected. Instead a dark line was found at locations where luminescences were missing.

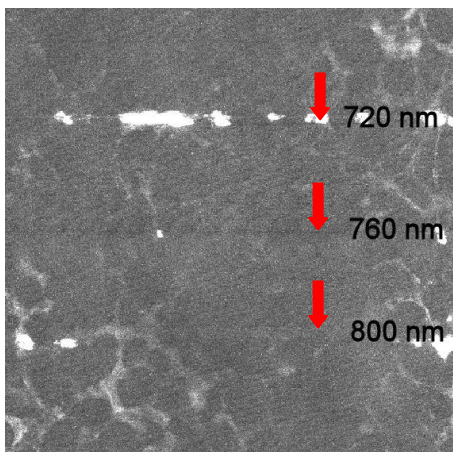


Fig. 34

Linear scans in a porcine cornea performed 48 hrs after extraction.

Excitation wavelengths for each line scan were indicated. Tissue depth was 70 μm . Luminescent elements were fewer as compared to fig. 34. Dark lines in the area of missing luminescent elements were much more common compared with fig. 33 as visible. The Chameleon™ laser was coupled to the LSM510-META™.

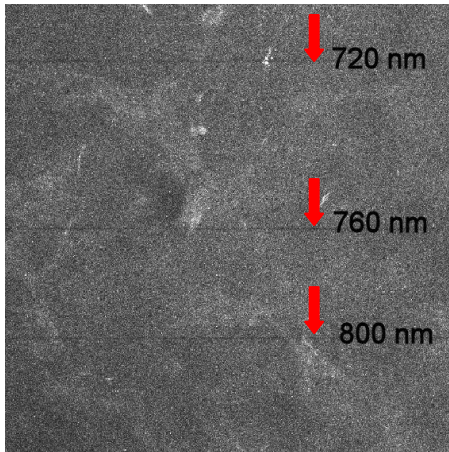


Fig. 35

Linear scans in a cornea diagnosed with keratoconus, 2 hrs after keratoplasty. Excitation wavelengths were indicated. Tissue depth was 70 μm . Dark lines appeared in the scanning area. No luminescent line was detected. The Chameleon™ laser was coupled to the LSM510-META™.

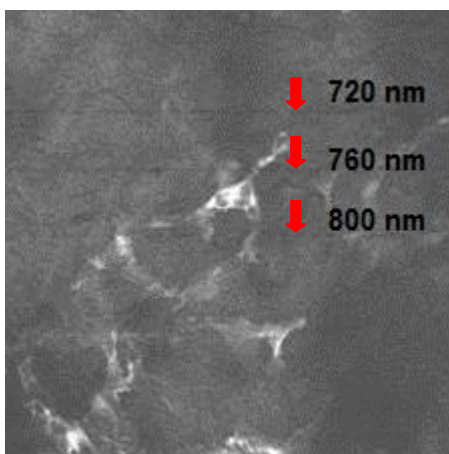


Fig. 36

Linear scans in a cornea diagnosed with keratoconus, 46 hrs after keratoplasty. Excitation wavelengths were indicated. Tissue depth was 70 μm . Dark lines appeared in the scanning area. As in the specimen obtained after 2 hrs (fig. 35), no

luminescent lines were found. The Chameleon™ laser was coupled to the LSM510-META™.

4.3.2. Dependence of lesion width on tissue depth

The purpose of this experiment was to compare lesion widths performed in different tissue depths using identical scanning parameters (fig. 37). In each selected level of tissue depth of the porcine cornea treated three linear scans were performed. The sample had been extracted ≤ 4 hrs before the experiment and was placed in cell medium and in a cell chamber during laser processing. The Vitesse™ laser was coupled to the LSM510-META™. The laser power at the target was 60 mW corresponding to a pulse energy of 0.75 nJ. Lesion width decreased with increasing tissue depth.

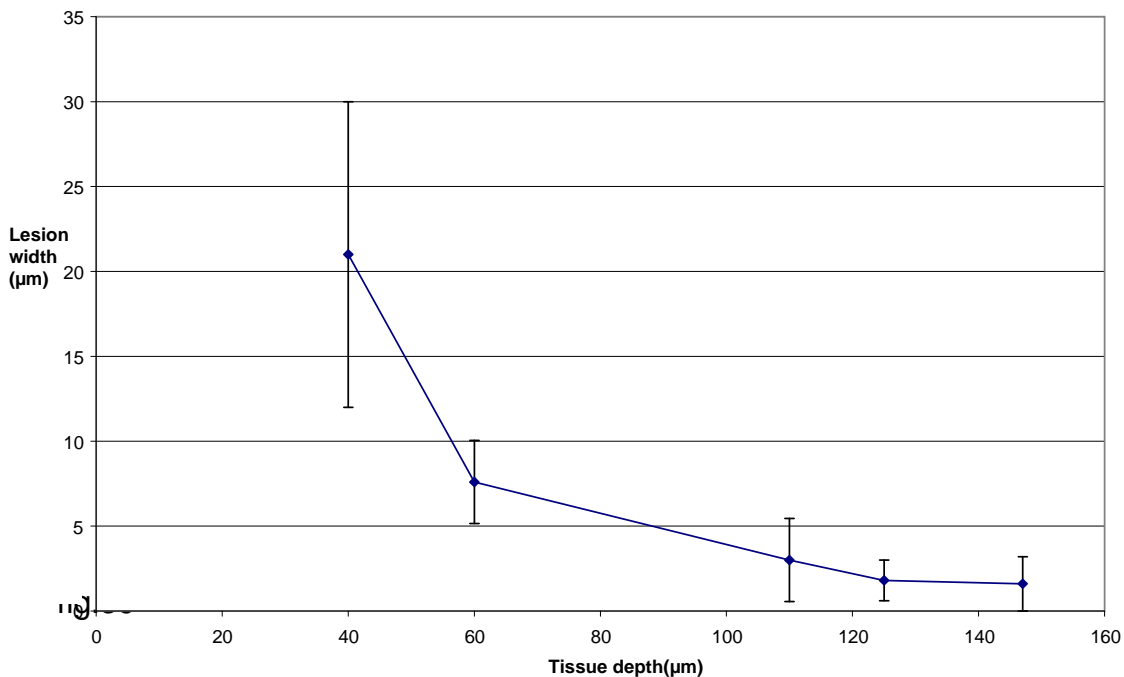


Fig. 37

Lesion width depending on tissue depth: Tissue depth was represented on the horizontal axis, lesion width on the vertical axis. Three linear scans were performed at each selected level of tissue depth and resulting luminescence was measured in 3 localizations determined by superposition of a grid.

Lesion width decreased with increasing tissue depth. The Vitesse™ laser was coupled to the LSM510-META™.

4.3.3. Dependence of lesion width on pulse energy

The purpose of this experiment was to measure the lesion width with pulse energy being increased (fig. 38). The setup included the Mai-Tai™ One Box laser coupled to the LSM510-META™. A tissue depth of $z = 100 \mu\text{m}$ was chosen in order to assure the intrastromal localization. The previously determined scanning time of 15 s was applied. A wavelength of 800 nm was used. Prior to measuring lesion widths for increasing powers at the target, a power threshold necessary to produce a visible stromal lesion of 65 mW was determined. The threshold was determined by increasing the laser power at the target up to the occurrence of a visible effect. Below this threshold, no laser effect was visible. The maximal power at the target available with this setup was 125 mW corresponding to a pulse energy of 1.5 nJ. Linear scans were performed intrastromally within two porcine corneas extracted ≤ 4 hrs before the experiment. The samples were placed in cell medium immediately after their extraction and for the whole duration of the experiment. The width of the plasma luminescence was measured at three standardized localizations within each line scan. Five line scans were performed for each laser power. Lesion width increased with increasing power at the target. Standard deviation increased as the laser power increased, indicating that plasma luminescence became more variable. All lesions had a width below $6 \mu\text{m}$.

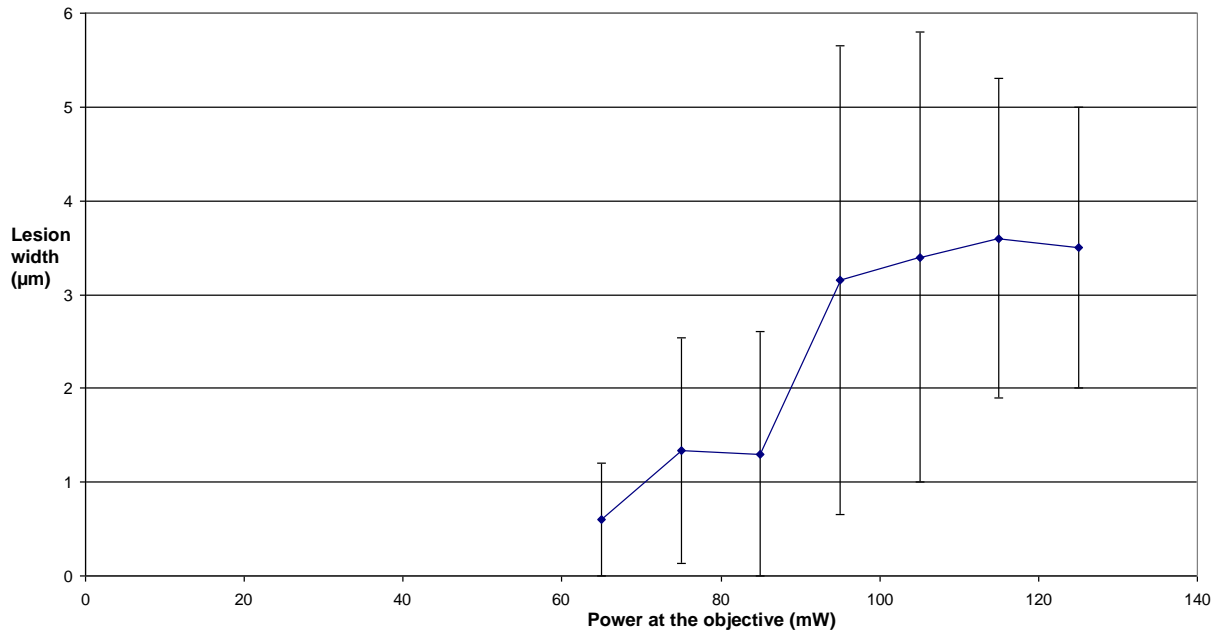


Fig. 38

Lesion width depending on laser power at the target:

Lesion width increased with increasing power at the target. 5 linear scans were performed at each chosen laser power at the objective. Luminescence was measured in 3 determined localizations by superposition of a grid. Standard deviation increased as the laser power increased, indicating that plasma luminescence became more variable. All lesions had a width below 6 µm. The Mai-Tai™ One Box laser was coupled to the LSM510-META™.

5. Discussion

5.1. Corneal imaging using autofluorescence and second harmonic generation

The widely tunable laser systems allowed easy switching between excitation wavelengths and permitted af and shg imaging (1, 22). Spatial focussing achieved by objectives with a high numeric aperture and time accumulation of laser energy in one femtosecond laser pulse provided laser power densities high enough to induce the simultaneous absorption of two photons. Laser energy was below 2 nJ. In previous studies, af signals had appeared particularly suitable to identify cellular structures while shg imaging displayed collagen structures. In this study, excitation wavelengths below 800 nm permitted visualization of cellular components, as cell nuclei and cell membranes were in strong contrast with cytoplasm. Keratocytes within the stroma were also showing a bright cytoplasm with darker nuclei and membranes. The cellular network including cell bodies and their branches could thus be described. At an excitation wavelengths of 800 nm or higher, cellular components were less clearly demarcated because of a weaker contrast between structures. However, shg signals were recorded arising from collagen. The arrangement of collagen lamellae within the stroma could be demonstrated. Epithelial cell layers were preferentially imaged in af. The imaging of the stroma seemed to benefit from both af and shg, as their combination allowed viewing all stromal components. Af and shg imaging delivered complementary information without the use of exogenous dyes. In order to obtain af images, endogenous fluorophores were required inside the tissue. Fluorophores were molecules capable of emitting spontaneous fluorescence. Mitochondria and to a less extent cell cytosol contained large amounts of the reduced coenzyme NAD(P)H which acted as endogenous fluorophores. They had a one-photon excitation wavelength of 340 nm and an emission wavelength between 450 and 470 nm (20). Consistent with this finding, these coenzymes could emit visible light, when excited with wavelengths in the near infrared and when assuming a two-photon-effect. Green or blue photons were emitted, in spite of the absorption of low energy, red photons. Cells like epithelial cells or fibrocytes contained a large number of coenzymes like NAD(P)H and thus their cytoplasm and especially their mitochondria became highly fluorescent and distinguishable from the

surroundings. Af imaging was preferable when the focus was on cellular detail. Knowing that the mentioned coenzymes were necessary for this “natural” fluorescence to occur, some limitations of the method became apparent. A sufficient quantity of these coenzymes appeared necessary. This implied a certain degree of vitality of the tissue. In the experiences described in this work, the intensity of the af signals decreased with time elapsed after the extraction of the sample, even when the sample was conserved in cell medium. Older ex vivo corneal samples could not be easily imaged by af. Furthermore, the imaging technique itself, based on the provocation of af, might have resulted in photobleaching and phototoxicity to the tissue. Thus, after excitation of a fluorescent molecule, the fluorophore itself might have been destroyed. In fact, an absorptive process occurred in af imaging: the simultaneous absorption of two photons, although of low-energy and occurring almost only within the focus. Tissue alteration and, possibly, damage to the surrounding tissue were inherent to this imaging mode. Shg imaging caused less damage to the tissue, as it involved no absorptive process, reducing phototoxicity and photobleaching. The patient’s cornea has always been mainly examined by slit-lamp microscopy in a clinical routine. More recently, confocal microscopy (e.g. HRT Rostock Kornea Modul, Heidelberg Engineering) and slit-lamp mounted OCT (e.g. SL-OCT, Heidelberg Engineering) were introduced to clinical practice. The described imaging technique allowed, just like confocal microscopy, a virtual slicing of corneal tissue in a pattern parallel to its surface, without previous alteration by exogenous dyes. However, confocal microscopes required a detection pinhole in order to exclude out-of-focus fluorescence, causing a deterioration of the picture. Multiphoton microscopy showed the advantage of producing af only within the focus. In fact, laser light intensities were sufficiently high to generate af only within the focal plane. Another disadvantage of confocal microscopy was the need for tissue contact, which might injure the patient. A distinctive feature of the multiphoton laser scanning microscope was its potential for therapeutic and diagnostic applications. Verification of the laser effects could immediately follow tissue manipulation. The use of lasers in the NIR allowed for imaging in quite a high tissue depth, due to the absence of natural absorbers and due to relatively weak tissue scattering. While interpreting the images acquired in LSM, some considerations had to be made. Other than the tissue alterations caused by the imaging technique itself and described above, the acquisition of the sample (during keratoplasty, during enucleation of the porcine

bulbi, during preparation of the porcine corneas, during transport) imposed a certain amount of trauma to the tissue. Subsequent examination of the tissue in light microscopy, examining influential parameters such as temperature, dehydration and mechanical irritation would be necessary. To allow for stress recovery, tissue should have been placed in cell medium overnight at a temperature of 4° C and examined in LSM the following day. Nevertheless, the intensity of the af signal was decreased the day after extraction of the sample and therefore, an early laser experiment was preferred. The importance of a correlative microscopy for improving the interpretation and the validation of LSM findings was already pointed out (27).

5.2. Imaging pathological cornea

The recognition of subtle cornea changes for example in slowly progressing keratoconus, in inflammatory disease or after refractive surgery is of a great clinical importance. Such changes could so far be detected only by confocal microscopy. Also allowing for images of subcellular detail, the described imaging techniques were applied to corneas diagnosed with keratoconus, Fuchs' endothelial dystrophy and herpes simplex keratitis. They represented frequent indications for corneal grafts. Morphological tissue abnormalities could be visualized. The thickness of the epithelial cell layer and the endothelial cell number could be determined with this method. However, in the examination of pathological samples, the very small field of vision (230 μm x 230 μm) and the relatively slow picture acquisition could have been considered a disadvantage. The acquired image could not only be described in terms of morphology, but could also be spectrally analyzed. In the case of a cornea diagnosed with keratoconus, such measurements were recorded (fig. 19 and 20). Collagen, an asymmetrical molecule, was known to emit wavelengths at half the incident wavelength, making it suitable for shg imaging. The background signal as reported in fig. 19 and 20 (circle) most likely corresponded to collagen. When exciting highly luminescent deposits detected in these images, a signal consisting of both half the incident wavelength (400 nm and 430 nm) as well as a diffuse signal throughout other wavelengths were registered. This finding could lead to the conclusion that these deposits consisted of collagen, but also of some other material, represented by the additional, diffuse signal. Since these changes were

found at the level of Bowman's layer, they might have resulted from a degenerative process. Although the exact nature of the luminescent elements could not be determined, a difference in the signal emitted by the luminescent areas compared to the darker surrounding area could be noted. Such registrations suggested that a spectral labelling of tissue constituents might be imaginable with this method, allowing for a spectral "recognition" of molecules. A higher number of samples would have to be imaged for this purpose. Also, a higher number may ensure that certain changes resulted from the pathology, not from the treatment preceding the experiment or from the experiment itself. Emphasis would have to be put on the correlation with other microscopic techniques, as light microscopy of this specimen revealed extensively damaged and dehydrated tissue.

A change of shape of epithelial cells (43) and in anterior collagen lamellae organization (31) were reported after af and shg experiences with keratokonus corneas. Furthermore, studies on corneal cross-linking have been performed (23, 42). Increased autofluorescence after the treatment was detected within the stroma. These observations demonstrated the potential of multiphoton microscopy in monitoring therapeutic effects.

5.3. Linear tissue ablation

A large amount of clinical experience with femtosecond lasers operating at pulse energies in the range of μJ was gained throughout the last years, especially in the field of refractive surgery. In femto-LASIK, the femtosecond laser was used to cut a flap while an UV excimer laser was ablating the stroma. The femtosecond laser was also increasingly introduced to corneal transplantation, for example for the creation of incisions in penetrating keratoplasty (10). Literature mostly presented experiences with femtosecond lasers operating at mJ or μJ pulse energies. Intrastromal tissue modeling using a femtosecond laser operating at a pulse energy of $1.3 \mu\text{J}$ was described in rabbit eyes, achieving central corneal thinning (28). In order to modify corneal tissue, the physical phenomenon of optical breakdown needed to be provoked. In corneal imaging as described above, the very low pulse energies (between 0.05 nJ and 0.2 nJ) were not sufficient to cause optical breakdown and visible tissue changes. Optical breakdown was a multiphoton effect, resulting from

non-linear multiphoton absorption and occurring at higher pulse energies. Optical breakdown was known to lead to either plasma-induced ablation (by means of plasma formation) or to photodisruption (by means of shock wave generation, cavitation and jet formation), or to both. Both plasma-induced ablation and photodisruption led to tissue ablation. The onset of plasma-induced ablation was known to occur at lower energy densities than the onset of photodisruption (32). This study showed a femtosecond laser system attaining the intensity threshold for optical breakdown with low pulse energies even below 1 nJ. High energy densities were achieved at rather low pulse energy by the simultaneous use of a high numeric aperture of the objective (above 1) and a high laser repetition frequency (above 100 MHz). The morphology of the effects of optical breakdown was observed after having parked the laser beam on a 230 μm line. A black line interrupted by luminescent elements appeared when applying different wavelengths at a pulse energy of 1.1 nJ. At a wavelength of 800 nm, the result of the linear scan was most consistent. In each cornea, imaging revealed a thin black line containing the smallest number of luminescent elements compared with the other laser parameters used. For this reason, an excitation wavelength of 800 nm was considered most suitable for tissue ablation. The black line lacking any fluorescent or luminescent element corresponded to an area of destructed tissue. The luminescent elements arose from plasma formation. Within the plasma, material could be eliminated due to high temperatures (21). Luminescent bubble-shaped elements formed, corresponding either to gas-filled bubbles or to cavitation bubbles. In order to distinguish between these bubbles, lifetime measurements of these elements are helpful. König et al (21) reported on small bubbles monitored during line scans with a laser power near the threshold for optical breakdown. Their relatively long lifespan corresponded to gas-filled bubbles rather than to short-lived cavitation bubbles. Interestingly, as seen in fig. 35-36, particular linear scans resulted in only a black line without evidence of plasma formation. Such black lines lacking luminescence could only be reproduced in older porcine tissue and in pathologic human cornea gained through keratoplasty, but not in fresh tissue. The exact development of these lines, showing no evidence of any plasma along their borders, remained unclear. Ding et al investigated the effects of micromachining lines into lightly fixed cat corneas at pulse energies between those for non-linear imaging and the optical breakdown threshold (7). They determined a pulse energy

of 0.3 nJ on average, for which lines could be micromachined without the appearance of bubbles or burns. They demonstrated the micromachined corneal changes under differential interference contrast imaging, causing a change in refractive index of the corneas. In this study, a threshold for optical breakdown was investigated at a tissue depth of 100 μm . A laser pulse energy of 0.8 nJ was necessary to achieve a visible effect (plasma formation) according to immediate verification in laser scanning microscopy. Around the threshold for optical breakdown (0.8 nJ) the resulting lesion width showed the smallest variability of width compared with other pulse energies tested. Therefore this particular pulse energy might be most advisable for tissue cutting. There was an unsteady tendency for an increasing lesion width with increasing laser pulse energy. Photodisruptive effects are known to be linearly dependent on pulse energy. In order to establish the diagram shown in fig. 38, only the lesion widths were measured. In order to examine the created lesions in light microscopy and eventually in electron microscopy, a sequence of linear scans was performed and epithelial marker lesions were created. However, in light microscopy the stroma appeared intact for all corneas. This observation suggested very little damage in surrounding tissue. In addition, tissue retraction could not be excluded.

5.4. Conclusion

Laser scanning microscopy was successfully applied to study corneal tissue and to determine morphologic and spectral characteristics in two photon excited autofluorescence and in second harmonic generation.

Tissue manipulation could be verified through the same system within seconds. Laser scanning microscopy revealed stromal tissue modification following the line scan, by changing the scan pattern from linear to frame and by adapting the laser power at the target. The system thus combined diagnostic and therapeutic applications in the management of corneal disease.

Cutting effects in corneal tissue as a function of age and condition of the specimen, laser wavelength, scanning time, tissue depth and power at the target were

investigated. Very precise tissue ablation could be performed without evidence of damage to surrounding tissue.

A setup allowing for larger intrastromal volumes to be treated would be needed in order to describe possible damage to adjacent tissue. Studies examining the side effects phototoxicity and photobleaching would be required in order to estimate the degree of damage suffered by vital cells. Further studies should aim at determining laser parameters which would be safe enough to apply to vital tissue.

6. References

1. Aptel F, Olivier N, Deniset-Besseau A, Legeais J, Plamann K, Schanne-Kleine M, Beaurepaire E: Multimodal nonlinear imaging of the human cornea. *Invest Ophthalmol Vis Sci* 2010; 51:2459-2465
2. Azar D, Ang R, Lee J, Kato T, Chen C, Jain S, Gabison E, Abad J: Laser subepithelial keratomileusis: electron microscopy and visual outcomes of flap photorefractive keratectomy. *Curr Opin Ophthalmol* 2001; 12:323-328
3. Bochert A, Berlau J, Koczan D, Seitz B, Thiessen H, Guthoff R: Genexpression bei Keratokonus. *Ophthalmologe* 2003; 100:545-549
4. Camellin M: Laser epithelial keratomileusis for myopia. *J Refract Surg* 2003; 19:666-670
5. Chayavichitsilp P, Buckwalter J, Krakowski A, Friedlander S: Herpes simplex. *Pediatr Rev* 2009; 30:119-129
6. Christopoulos V, Kagemann L, Wollstein G, Ishikawa H, Gabriele M, Wojtkowski M, Srinivasan V, Fujimoto J, Duker J, Dhaliwal D, Schuman J: In vivo corneal high-speed, ultra-high-resolution optical coherence tomography. *Arch Ophthalmology* 2007; 125:1027-1035
7. Ding L, Knox W, Bühren J, Nagy L, Huxlin K: Intratissue refractive index shaping (IRIS) of the cornea and lens using a low-pulse-energy femtosecond laser oscillator. *Invest Ophthalmol Vis Sci* 2008; 49:5332-5339
8. Drexler W, Morgner U, Ghanta R, Kärtner F, Schuman J, Fujimoto J: Ultrahigh-resolution ophthalmic optical coherence tomography. *Nat Med* 2001; 7:502-507
9. Erie J: Corneal wound healing after photorefractive keratectomy: a 3-year confocal microscopy study. *Trans Am Ophthalmol Soc* 2003; 101:287-328
10. Farid M, Steinert R: Femtosecond laser-assisted corneal surgery. *Curr Opin Ophthalmol* 2010; 21:288-292
11. Fayol N, Labbé A, Dupont-Monod S, Dupas B, Baudouin C: Apport de la microscopie confocale in vivo et de la tomographie en cohérence optique de chambre antérieure pour l'étude de pathologies endothéliales cornéennes. *J Fr Ophtalmol* 2007; 30:348-356
12. Göppert-Mayer M: Über Elementarakte mit zwei Quantensprüngen. *Ann Phys* 1931; 9:273-295
13. Gwon A: Prospective evaluation of radial keratotomy (PERK) study 10 years after surgery. *Arch Ophthalmol* 1995; 113:1225-1226
14. Hamilton D, Johnson R, Lee N, Bourla N: Differences in the corneal biomechanical effects of surface ablation compared with laser in situ keratomileusis using a microkeratome or femtosecond laser. *J Cataract Refract Surg* 2008; 34:2049-2059
15. Holland E, Schwartz G: Classification of herpes simplex virus keratitis. *Cornea* 1999; 18:144-154
16. Kanski J (ed) (2003) *Clinical Ophthalmology. A Systematic Approach*. 5th ed. Butterworth-Heinemann, Edinburgh London New York Oxford Philadelphia St Louis Sydney Toronto

17. Kezirian G, Stonecipher K: Comparison of the IntraLase femtosecond laser and mechanical keratomes for laser in situ keratomileusis. *J Cataract Refract Surg* 2004; 30:804-811
18. Kim P, Sutton G, Rootman S: Applications of the femtosecond laser in corneal refractive surgery. *Curr Opin Ophthalmol* 2011; 22:238-244.
19. König K: Laser tweezers and multiphoton microscopes in life sciences. *Histochem Cell Biol* 2000; 114:79-92
20. König K, Wollina U, Riemann I, Peuckert C, Halbhuber K, Konrad H, Fischer P, Fünfstück V, Fischer T, Elsner P: Tomography of human skin with subcellular spatial and picosecond time resolution using intense near infrared femtosecond laser pulses. *SPIE-Proceedings* 2002; 4620: 191-201
21. König K: High-resolution multiphoton imaging and nanosurgery of the cornea using femtosecond laser pulses. In: Fankhauser F, Kwasniewska S (eds) *Lasers in Ophthalmology - Basic, Diagnostic and Surgical Aspects*. Kugler Publications, The Hague, 2003 pp 79-89
22. Krüger A, Hovakimyan, Ramirez D, Stachs O, Lubatschowski H, Wree A, Guthoff R, Heisterkamp A: Farbstofffreie Zweiphotonenmikroskopie der Augenhornhaut. *Klin Monatsbl Augenheilkd* 2009; 226:970-979
23. Krüger A, Hovakimyan M, Ramirez D, Stachs O, Wree A, Guthoff R, Heisterkamp A: Combined nonlinear and femtosecond confocal laser-scanning microscopy of rabbit corneas after photochemical cross-linking. *Invest Ophthalmol Vis Sci* 2011; 52:4247-4255
24. Kubota T, Seitz B, Tetsumoto K, Naumann G: Lamellar excimer laser keratoplasty: reproducible photoablation of corneal tissue. A laboratory study. *Doc Ophthalmol* 1992; 82:193-200
25. Lamparter J, Dick H, Krummenauer F. Complications after laser in situ keratomileusis (LASIK): Results of a meta-analysis on incidences and expectable costs. *Klin Monatsbl Augenheilkd* 2007; 224:627-635.
26. Masters B, Böhnke M: Three-dimensional confocal microscopy of the human cornea in vivo. *Ophthalmic Res* 2001; 33:125-135
27. Masters B: Correlation of histology and linear and nonlinear microscopy of the living human cornea. *J Biophotonics* 2009; 2:127-139
28. Meltendorf C, Deller T, Ackermann H, Von Pape U: Corneal intrastromal tissue modeling with the femtosecond laser. *Graefes Arch Clin Exp Ophthalmol* 2011; 249:1661-1666
29. Minsky M: Memoir on inventing the confocal microscope. *Scanning* 1988; 10:128-138
30. Mohler W, Millard A, Campagnola P: Second harmonic generation imaging of endogenous structural proteins. *Methods* 2003; 29:97-109
31. Morishige N, Wahlert A, Kenney M, Brown DJ, Kawamoto K, Chikama T, Nishida T, Jester J: Second-harmonic imaging microscopy of normal human and keratoconus cornea. *Invest Ophthalmol Vis Sci* 2007; 48:1087-1094
32. Niemz M (2002) *Laser-Tissue Interactions. Fundamentals and Applications*. 2nd rev ed. Springer, Berlin Heidelberg New York
33. Pallikaris I, Papatzanaki M, Stathi E, Frensch O, Georgiadis A. Laser in situ keratomileusis. *Lasers Surg Med* 1990; 10:463-468.
34. Patel S, Maguire L, McLaren J, Hodge D, Bourne W: Femtosecond laser versus mechanical microkeratome for LASIK. A randomized controlled study. *Ophthalmology* 2007; 114:1482-1490

35. Sakimoto T, Rosenblatt M, Azar D. Laser eye surgery for refractive errors. *Lancet* 2006; 367:1432-1447
36. Sarayba M, Ignacio T, Binder PS, Tran DB: Comparative study of stromal bed quality by using mechanical, IntraLase femtosecond laser 15- and 30-kHz microkeratomes. *Cornea* 2008; 26:446-451
37. Schiebler T, Schmidt W, Zilles K (1999) *Anatomie*. 8. Aufl. Springer, Berlin Heidelberg New York
38. Seiler T, Wollensak J: Myopic photorefractive keratectomy with the excimer laser. One-year follow-up. *Ophthalmology* 1991; 98:1156-1163
39. Seiler T: The Excimer laser. An instrument for corneal surgery. *Ophthalmologie* 1992; 89:128-133
40. Seitz B, Langenbucher A, Nguyen N, Kus M, Kuchle M, Naumann G: Results of the first 1,000 consecutive elective nonmechanical keratoplasties using the excimer laser. A prospective study over more than 12 years. *Ophthalmologie* 2004; 101:478-488
41. Srinivasan R: Ablation of polymers and biological tissue by ultraviolet lasers. *Science* 1986; 234:559-565.
42. Steven P, Hovakimyan M, Guthoff R, Hüttmann G, Stachs O: Imaging corneal crosslinking by autofluorescence 2-photon microscopy, second harmonic generation, and fluorescence lifetime measurements. *J Cataract and Refract Surg* 2010; 36:2150-2159
43. Tan H, Sun Y, Lo W, Lin S, Hsiao C, Chen Y, Huang S, Lin W, Jee S, Yu H, Dong C. Multiphoton fluorescence and second harmonic generation imaging of the structural alterations in keratoconus ex vivo. *Invest Ophthalmol Vis Sci* 2006; 47:5251-5259
44. Tasman W, Jaeger E (eds) (2003): *Duane's Clinical Ophthalmology on Cd-Rom*. 2003 ed. Lippincott Williams & Wilkins, Philadelphia
45. Teng S, Tan H, Peng J, Lin H, Kim K, Lo W, Sun Y, Lin W, Lin S, Jee S, So P, Dong C: Multiphoton autofluorescence and second-harmonic generation imaging of the ex vivo porcine eye. *Invest Ophthalmol Vis Sci* 2006; 47:1216-1224
46. Touboul D, Salin F, Mortemousque B, Chabassier P, Mottay E, Léger F, Colin J: Avantages et inconvénients du microkératome laser femtoseconde. *J Fr Ophtalmol* 2005; 28:535-546
47. Visser N, McGhee C, Patel D: Laser scanning in vivo confocal microscopy reveals two morphologically distinct populations of stromal nerves in normal human cornea. *Br J Ophthalmol* 2008; 93:506-509
48. Waring G 3rd, Lynn M, McDonnell P: Results of the prospective evaluation of radial keratotomy (PERK) study 10 years after surgery. *Arch Ophthalmol* 1994; 112:1298-1308
49. Wilson R, Roper-Hall M: Effect of age on the endothelial cell count in the normal eye. *Br J Ophthalmol* 1982; 66:513-515
50. Wirbelauer C (2006): *Die Entwicklung der Optischen Kohärenz-Tomographie der Hornhaut*. Dissertation. FU Berlin.
51. Wojtyczka E, Szaflik J: The history of correction of refractive errors: refractive surgery. *Arch Hist Filoz Med* 2000; 63:249-257
52. Zoumi A, Yeh A, Tromberg B: Imaging cells and extracellular matrix in vivo by using second-harmonic generation and two-photon excited fluorescence. *Appl Biol Sci* 2002; 99:11014-11019

7. Publikationen

Vortrag: Huss C, Schirra F, Gatzioufas Z, Seitz B: "Avastin – Augentropfen bei kornealen Neovaskularisationen". 80. Versammlung der Rhein-Mainischen Augenärzte, Frankfurt am Main, 2007

Poster: Huss C, Riemann I, König K, Laue M, Mestres P, Löw U, Hild M, Ruprecht KW, Krause MHJ: " Experimental corneal imaging and intrastromal tissue ablation with femtosecond laser scanning microscopy". ARVO Annual Meeting, Fort Lauderdale, Florida, 2005

Poster: Troeber L, Krause M, Huss C, Riemann I, Seitz B, Mestres P, Hild M, König K: „Bildgebung mit Laser-Scanning-Mikroskopie (LSM) bei kornealem intrastromalen Gewebeabtrag mit unverstärkten Femtosekunden-Laserpulsen in-vitro“. 104. Jahrestagung der DOG, Berlin, 2006

Poster: Hild M, Löw U, Laue M, Mestres P, Huss C, Ruprecht K, Krause M, Riemann I, König K: „Experimental retinal ablation and imaging with femtosecond laser pulses“. ARVO Annual Meeting, Fort Lauderdale, Florida, 2005

Vortrag: Krause M, Löw U, Mestres P, Huss C, Hild M, Riemann I, Ruprecht K, Laue M, Jahn S, König K: „Experimentelle Hornhautchirurgie mit Femtosekundenlaser“. 77. Versammlung der Rhein-Mainischen Augenärzte, Homburg, 2004

8. Danksagung

Herrn Prof. Dr. Berthold Seitz, F.E.B.O. danke ich für die Unterstützung dieser Arbeit.

Herrn Prof. emer. Dr. Klaus Wilhelm Ruprecht danke ich für die Unterstützung in der Anfangsphase des Projektes.

Herrn Prof. Dr. Matthias Krause danke ich für die Überlassung des Themas und für die zuverlässige Betreuung.

Herrn Prof. Dr. Karsten König danke ich für die Übermittlung von Kenntnissen über die Multiphotonenmikroskopie und für die Möglichkeit der Mitarbeit im Labor.

Frau Dr. Iris Riemann, Herrn Dr. Frank Stracke und Herrn Dr. Ronan Le Harzic danke ich für die ausgezeichnete Beratung bei theoretischen und praktischen Fragen im Labor.

Herrn Prof. emer. Dr. Dr. Pedro Mestres danke ich für seine Erläuterungen zur mikroskopischen Anatomie und für zahlreiche hilfreiche Vorschläge.

Herrn PD Dr. Konrad Hille danke ich für seine Kooperation bei der Gewinnung des Gewebes.

Herrn Daniel Sauer danke ich für die technische Hilfe bei der Nutzung der Laser.

Frau Birgit Leis und Frau Gabi Kiefer danke ich für die Assistenz bei der Anfertigung histologischer Präparate.

Ein besonderer Dank gilt meinen Eltern. Sie haben mir das Studium und diese Arbeit ermöglicht.